Applied Geochemistry xxx (20xx) xxxxxx

Contents lists available at ScienceDirect

Applied Geochemistry

journal homepage: www.elsevier.com/locate/apgeochem

Trace and rare earth element distribution in hyperalkaline serpentinite-hosted spring waters and associated authigenic carbonates from the Ronda peridotite

Jennifer Zwicker [a,*], Daniel Smrzka [b,c], Iñaki Vadillo [d], Pablo Jiménez-Gavilán [d], Manolis Giampouras [e], Jörn Peckmann [f], Wolfgang Bach [b,c]

[a] Institut für Mineralogie und Kristallographie, Universität Wien, 1090, Wien, Austria
[b] MARUM-Center of Marine and Environmental Sciences, 28359, Bremen, Germany
[c] Geoscience Department, University of Bremen, 28359, Bremen, Germany
[d] Group of Hydrogeology, Department of Geology and Ecology, University of Malaga, 29071, Malaga, Spain
[e] Andalusian Institute of Earth Sciences (IACT), 18100 Armilla, Granada, Spain
[f] Institut für Geologie, Centrum für Erdsystemforschung und Nachhaltigkeit, University of Hamburg, 20146, Hamburg, Germany

ARTICLE INFO

Editorial handling by Dr F Chabaux

Keywords:
Hyperalkaline springs
Ronda peridotite
Authigenic carbonates
Rare earth elements
Geochemical modeling

ABSTRACT

The Ronda peridotite in southern Spain is subject to low-temperature serpentinization by circulating groundwaters that produces hyperalkaline fluids of high pH and low dissolved inorganic carbon content (DIC). When these waters resurface as hyperalkaline springs they take up atmospheric carbon dioxide (CO_2), which triggers the precipitation of travertine carbonates. Spring waters at Baños del Duque, Fuente Romana, and Fuente Amargosa show typical chemical features of hyperalkaline springs such as high pH and low DIC, yet exhibit an unusual distribution of rare earth elements (REEs) enriched in lanthanum (La) and cerium (Ce). In order to constrain changes in spring water chemistry and carbonate precipitation during atmospheric CO_2 uptake, a reaction path model was set up to illustrate that the distribution of REE species in the high pH and low DIC water is strongly dependent on REE complexation by hydroxide and carbonate species. Reaction path modeling results show that during spring fluid emission and CO_2 uptake, REE speciation in the fluids shifts from a dominance of hydroxide to carbonate complexes. The complexation of rare earth elements in the high pH, low DIC fluids strongly depends on the DIC content of the respective fluid. The REE distribution of travertine deposits associated with the hyperalkaline springs deviates from that in the fluids, suggesting that travertines precipitated from fluids different to those currently emitted from the springs.

1. Introduction

Low-temperature serpentinization of ultramafic rocks exposed on Earth's surface is a timely topic of research due to its potential for carbon capture and storage strategies (Kelemen et al., 2011; Klein and McCollom, 2013; Schwarzenbach et al., 2013a), as well as for its potential to host subsurface ecosystems entirely independent of photosynthesis (Russell et al., 2010; McCollom and Seewald, 2013; Zwicker et al., 2018a; Glombitza et al., 2021). Since the discovery of low-temperature serpentinite-hosted ecosystems on the seafloor (Kelley et al., 2005), a large number of analogous environments on land have been investigated worldwide (Barnes et al., 1978; Neal and Stanger, 1985; Neal and Shand, 2002; Blank et al., 2009; Chavagnac et al., 2013a; Schwarzenbach et al., 2013b; Szponar et al., 2013; Morrill et al., 2014; Meyer-Dombard et al., 2015; Etiope et al., 2016; Giampouras et al., 2019, 2020; Templeton et al., 2021). Low-temperature serpentinization of uplifted and exposed ultramafic rocks such as mantle peridotites proceeds through the percolation of meteoric water, allowing for water-rock interactions to produce fluids with unique chemical composition (Neal and Stanger, 1984). These fluids evolve into two fluid types based on their pH and concentrations in calcium (Ca), magnesium (Mg), and dissolved inorganic carbon (DIC): The type-I waters which show mildly alkaline pH of 8–9, low Ca, high Mg and bicarbonate concentrations, and the type-II waters characterized by a high pH up to 12, low Mg, DIC, and high Ca concentrations (Barnes et al., 1967; Barnes and O'Neil, 1969; Paukert et al., 2012; Mervine et al., 2014). Type I waters circulate through the

* Corresponding author.
E-mail address: jennifer.zwicker@univie.ac.at (J. Zwicker).

https://doi.org/10.1016/j.apgeochem.2022.105492
Available online 31 October 2022

shallow bedrock and are in contact with the atmosphere, which provides a carbon source via the diffusion of carbon dioxide (CO_2; Barnes and O'Neil, 1971; Bruni et al., 2002). Groundwater percolating deeper into the subsurface gradually becomes isolated from the atmosphere and evolves into type-II fluids. Magnesium and Ca are exchanged during the hydration of minerals including olivine, pyroxene, and diopside (Bruni et al., 2002; Miller et al., 2016). Although both Mg and Ca are leached from the minerals, Mg is incorporated into secondary minerals such as chrysotile, talc, and brucite, as well as Mg-rich carbonates, while Ca accumulates in the residual fluid (Barnes et al., 1967; Bruni et al., 2002; Cipolli et al., 2004; Paukert et al., 2012). The type-II waters are therefore left with high Ca concentrations and very high pH of up to 12 (Neal and Stanger, 1984, 1985), and can resurface as hyperalkaline springs (Barnes and O'Neil, 1969; Neal and Stanger, 1985; Bruni et al., 2002). Hyperalkaline spring discharge at the surface induces the precipitation of travertine carbonates via the rapid uptake of atmospheric CO_2 into the high-pH, low-DIC fluids (Neal and Stanger, 1985; Clark and Fontes, 1990; Clark et al., 1992).

The rare earth elements (REEs) are a series of elements that show similar geochemical behavior, and allow for the reconstruction of environmental conditions in natural waters (Elderfield and Sholkovitz, 1987; Elderfield et al., 1990; Tang and Johannesson, 2003; Abbott et al., 2015). Despite their similar behavior, small differences among the REEs lead to fractionation depending on the speciation and complexation of the individual elements and water chemistry (Sholkovitz et al., 1994). The light, middle, and heavy REEs (LREEs, MREEs, and HREEs, respectively from hereon) form complexes of different strength with anions of high electronegativity such as dissolved hydroxide, carbonate, sulfate, chloride, phosphate, and fluoride species (Cantrell and Byrne, 1987; Wood, 1990; Lee and Byrne, 1993; Luo and Byrne, 2001, 2004). Complexation additionally depends on pH, Eh, salinity, temperature, and concentration of potential ligands in solution, controlling the REE distribution in marine (De Baar et al., 1991; Bach et al., 2003; Schijf et al., 2015) and terrestrial environments (Möller and Bau, 1993; Johannesson and Lyons, 1994a; 1995b; Serrano et al., 2000). Dissolved REEs are easily incorporated into solid phases that precipitate from parent fluids such as carbonates and phosphates, in which they are widely used as archives for past and present environmental conditions (Sholkovitz and Shen, 1995; Webb and Kamber, 2000; Lécuyer et al., 2004; Smrzka et al., 2019).

Here we provide the first detailed investigation of REE distribution and speciation in hyperalkaline springs associated with onshore, low-temperature serpentinization in the Ronda peridotite, which is one of the largest outcrops of subcontinental mantle peridotite worldwide (Tubia et al., 1997). The unique chemistry of the discharging spring waters produces an unusual distribution of REEs, controlled by a combination of solution pH and dissolved carbon concentrations. Travertine carbonates precipitating in the course of spring discharge are considered efficient scavenging agents of REEs, as well as of potentially toxic trace elements (Casanova et al., 1999; Winkel et al., 2013; Khoury et al., 2014; Olsson et al., 2014; Teboul et al., 2016). Using a comprehensive approach including trace and rare earth element geochemistry of spring waters and associated carbonates, as well as hydrogeochemical modeling, the first-order constraints of REE speciation in spring waters and their uptake from parent fluids by the precipitating minerals are determined.

2. Geologic setting and hyperalkaline springs

The Ronda peridotite is part of the Betic Cordillera mountain range, and represents the largest outcrop of exposed subcontinental mantle peridotite (Fig. 1, Lenoir et al., 2001). Rocks of the Ronda peridotite crop out over an area of over 450 km^2, and consist mostly of lherzolite with subordinate harzburgite and dunite, as well as accessory garnet-spinel- and plagioclase pyroxenites (Suen and Frey, 1987; Garrido et al., 2011). The Ronda peridotite is one of several Neogene emplacements of Alpine orogenic rocks that developed since the late Mesozoic, and were exhumed and emplaced during the earliest Miocene as a 1.5-km-thick overthrust sheet onto carbonates and metapelites of the Sierra de las Nieves and Blanca-Mijas mountain ranges (Van der Waal and Vissers, 1996; Platt et al., 2003). The Ronda peridotite is known for its variety of circumneutral to hyperalkaline springs, of which over 70 have been documented to date (Vadillo et al., 2015; Etiope et al., 2016). Meteoric precipitation fuels groundwater recharge, enabling groundwater circulation through the ultramafic body and its discharge to the surface as hyperalkaline springs (Etiope et al., 2016). The emitted groundwaters are typical type II Ca – hydroxide (OH)-rich waters produced by chemical interactions with ultramafic deep-seated rocks (Giampouras et al., 2019). They are poor in Mg, rich in Na, K, Ca, and Cl, feature high pH of up to 12, and induce travertine formation via discharge and reaction with atmospheric CO_2 and/or mixing with type I Mg–HCO_3-rich river water (Giampouras et al., 2019).

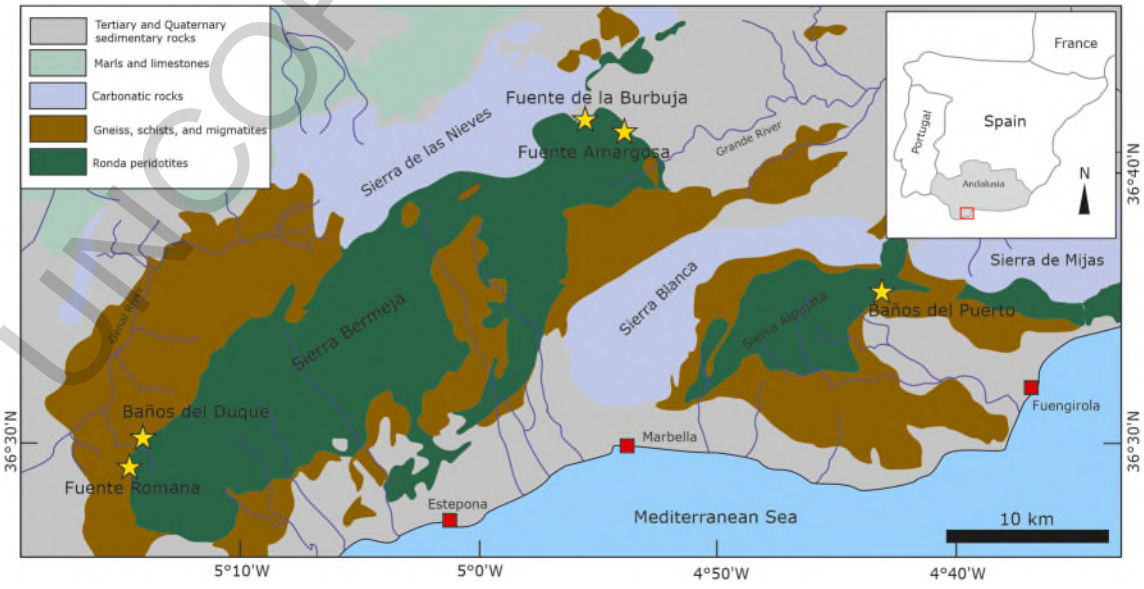

Fig. 1. Overview of the study areas within the Ronda peridotite, southern Spain.

3. Material and methods

3.1. Hydrochemistry

Water and travertine samples were collected during field trips from two categories of springs previously described in detail in Etiope et al. (2016) and Giampouras et al. (2019). Three spring sites of the first category, Baños del Duque (BD), Fuente Romana (FR), and Fuente Amargosa (FA) (Fig. 1), were selected because of the highly alkaline nature of emitting waters with a high pH and low DIC contents. A fourth spring corresponding to the second category, Fuente de la Burbuja (FB) near the town of Tolox was sampled for comparison due to its circumneutral water chemistry and higher DIC content (Fig. 1). Sterile high-density polyethylene bottles (120 mL) sealed with inverted cone caps were used to store water samples for hydrochemical analyses. All water samples were filtered through a 0.45 μm Millipore® (Merck KGaA, Darmstadt, Germany) filter. Bottles were rinsed before sampling, carried in a cool-box and stored in a fridge (<4 °C) until analysis, generally performed within 24 h after sampling. A portable multi-parameter probe (Hach-Lange HQ40d; Hach, Loveland, CO, USA) was used to measure *in situ* physicochemical parameters: pH, temperature, dissolved oxygen (DO) and electrical conductivity (EC). pH was calibrated with 7 and 10 buffer solutions the same day of sampling. Chemical analyses of major and minor ions (Ca^{2+}, Mg^{2+}, Na^{+}, K^{+}, HCO_3^-, CO_3^{2-}, Cl^-, SO_4^{2-}, and NO_3^-) were conducted at the laboratory of the Center for Hydrogeology of the University of Málaga, Spain. Alkalinity (HCO_3^-, CO_3^{2-}, and OH^-) was determined with a titration analyzer Systems (888 Titrando Metrohm®) and other ions were determined using a Metrohm® 881 Compact IC Pro (HPLC). Chemical parameters and major and minor ion concentrations in spring waters are shown in Table 1. Rare earth element concentrations in spring waters were determined by ICP-MS in the geochemical laboratory of the Jacobs University of Bremen following the method of Schmidt et al. (2019) and references therein. Rare earth element concentrations in spring waters are shown in Table 2.

3.2. Petrography, mineralogy, and geochemistry of carbonates

Carbonate samples from BD were collected from crusts in proximity to the spring discharge close to a small stream (Fig. 2A). Carbonate samples from Baños del Puerto (BP) were taken from crusts directly at the spring discharge (Fig. 2B), as well as from travertine precipitated from formerly active spring water streams close to the discharge site (Fig. 2C). Thin sections of carbonate samples from BD and BP springs sites were prepared at the Institute of Geology of the University of Vienna. Thin section petrography was performed on a Leica DM4500 P polarization microscope, and photomicrographs were taken using a Leica DFC 450 C camera using the Leica Application Suite 4.4.0 software for image analysis and camera control. Powdered samples from carbonate crusts and slabs were obtained by crushing the specimen with a hammer and grinding it to a fine powder using an agate pestle and mortar. Carbonate powders were analyzed with a Panalytical PW 3040/60 X'Pert PRO (CuKα radiation, 40 kV, 40 mA, step size 0.0167, 5 s per step) diffractometer at the Institute of Geology at the University of Vienna. The X-ray diffraction patterns were interpreted using the software "X'Pert High score plus" (Panalytical).

Major, trace, and rare earth elements of carbonates in thin sections were determined with laser ablation inductively coupled plasma mass spectrometry (LA-ICP-MS) using a NewWave UP 193 nm solid-state laser coupled to a Thermo-Finnigan Element 2 HR-ICP-MS at the University of Bremen. The use of a laser wavelength of 193 nm is well suited for carbonates as it produces more uniform ablation yields, reduced matrix effects, and yields better reproducibility between multiple analyses compared to lasers of a higher wavelength (Günther and Heinrich, 1999; Guillong et al., 2003; Jochum et al., 2012). Pre-ablation was conducted with a beam diameter slightly larger than the beam diameter used for the actual measurement and 5 Hz pulse rate prior to analysis. Samples and standards were ablated with an irradiance of approximately 1 GW cm^{-2}, spot sizes of 35–100 μm, and a laser pulse rate of 5 Hz. Plasma power was 1200 W, helium (approximately 0.8 L min^{-1}) was used as sample gas, and argon (approximately 0.8 L min^{-1}) was subsequently added as make-up gas. All isotopes were analyzed at low resolution with 5 samples in a 20% mass window and a total dwell time of 25 ms for each isotope. Blanks were measured for 20 s prior to ablation. After every 5 to 10 samples NIST610 glass was analyzed as external calibration standard using the values of Jochum et al. (2011). The Cetac GeoPro™ software was used for data quantification and ^{43}Ca was used as the internal standard. The interference of $^{86}Sr^{2+}$ on $^{43}Ca^{+}$ was corrected for all carbonate analyses using a factor derived from regular analyses of a Sr-rich carbonate standard (MACS-3). All major elements were recalculated to their oxide (aluminum (Al), silicon (Si)) or carbonate (Mg, Ca, manganese (Mn), iron (Fe), strontium (Sr)) form, respectively and normalized to 100%. Data quality was assessed by regular analyses of USGS reference materials BCR-2G and BHVO-2G (basaltic glasses) along

Table 1
Main chemical parameters of hyperalkaline spring fluids from Baños del Duque, Fuente Romana, Fuente Amargosa, and circumneutral fluids from Fuente de la Burbuja. TOC = total organic carbon. All data in mgL^{-1}, *in μS cm^{-1}, **in °C, ***as HCO_3^- in mgL^{-1} for Fuente de la Burbuja, and as CO_3^{2-} in mgL^{-1} for Baños del Duque, Fuente Romana, and Fuente Amargosa.

	Baños del Duque	Fuente Romana	Fuente Amargosa	Fuente de la Burbuja
pH	10.96	11.62	11.29	7.69
Electric conductivity*	559	559	1240	445
Temperature**	16.3	13.7	17.1	n.d.
O_2	1.73	2.40	2.49	8.83
DIC***	13.2	17.0	34.1	299
$Alkalinity_{CaCO_3}$	165	176	368	489
TOC	0.278	0.140	2.25	0.461
Ca^{2+}	32.0	33.1	52.2	53.5
Mg^{2+}	0.048	0.020	0.350	36.2
Na^{+}	32.7	25.4	83.5	3.39
K^{+}	4.24	3.85	10.19	0.580
Si	3.15	4.70	2.14	6.8
F^-	0.071	n.d.	0.180	0.404
Cl-	33.5	22.2	71.1	5.12
NO_2^-	n.d.	n.d.	n.d.	0.139
Br^-	0.478	n.d.	0.540	n.d.
NO_3^-	0.772	n.d.	0.740	2.06
SO_4^{2-}	6.83	3.27	4.35	6.45

Table 2
Dissolved rare earth elements of hyperalkaline spring fluids from Baños del Duque, Fuente Romana, Fuente Amargosa, and circumneutral fluids form Fuente de la Burbuja. All data in ng kg^{-1}.

	Baños del Duque	Fuente Romana	Fuente Amargosa	Fuente de la Burbuja
La	40.8	50.1	38.3	7.11
Ce	24.1	28.6	31.7	11.8
Pr	0.583	0.618	1.99	1.35
Nd	2.48	2.49	8.75	5.34
Sm	0.657	0.589	2.50	1.11
Eu	0.175	0.158	0.768	0.294
Gd	0.763	0.66	2.80	1.21
Tb	0.763	0.653	2.80	1.07
Dy	0.674	0.537	2.05	1.05
Y	3.54	2.77	9.49	7.31
Ho	0.129	0.099	0.360	0.196
Er	0.359	0.270	0.936	0.598
Tm	spike	spike	spike	spike
Yb	0.292	0.223	0.708	0.519
Lu	0.041	0.029	0.092	0.074
∑REE + Y	75.4	87.7	103	39.0

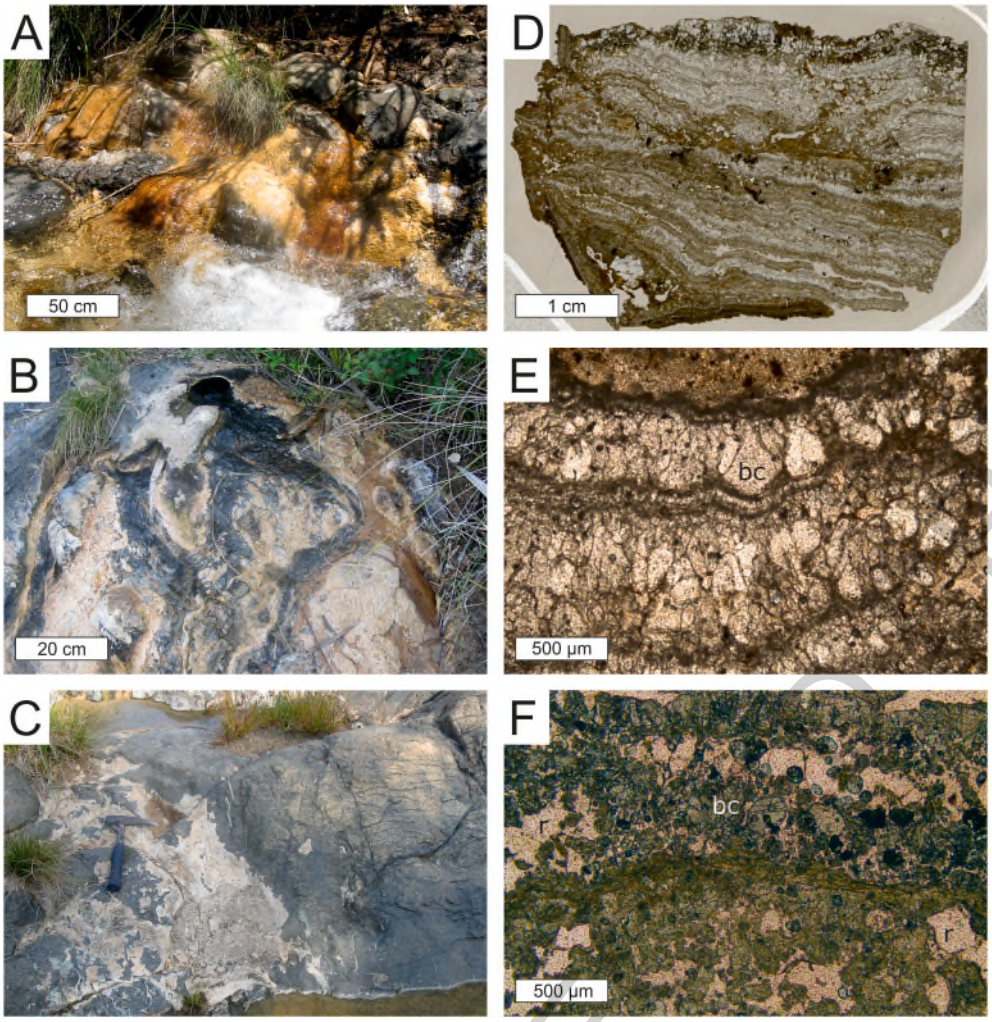

Fig. 2. (A) Outcrop photograph of the travertine from Baños del Duque. (B) Outcrop photograph of the travertine deposits around the spring discharge site at Baños del Puerto. (C) Outcrop photograph of the travertine deposits from Baños del Puerto, size of the hammer is 29 cm. (D) Thin section scan of Baños del Puerto travertine. (E) Photomicrograph of Baños del Puerto travertine carbonate featuring horizontal bands of blocky calcite (bc). (F) Photomicrograph of Baños del Duque travertine with blocky calcite (bc), r = resin.

with the samples. Measurement accuracy was better than 7% except for Zn, Ti, Sb, and As, and precision was better than 5.5% except for As, Sb, and Re. Because the detection limits of the REEs and Y were not well defined owing to their low blanks, a detection limit of 0.001 µg g^{-1} was assigned. Such low contents for some elements correspond to very few counts per second resulting in relative standard deviations as high as 60%. All quantified data are shown in Tables 3 and 4, but we note that values below approximately 0.02 mg kg^{-1} are close to the detection limits. Rare earth element contents of carbonates were normalized to Post Archean Australian Shale (PAAS) after McLennan (1989).

3.3. Geochemical modeling

The Geochemists Workbench software package (Bethke, 2005) was used in order to calculate REE speciation in hyperalkaline and circumneutral Ronda spring waters. Equilibrium constants for the formation of aqueous complexes of REEs were taken from the SOLTHERM database (https://pages.uoregon.edu/palandri/data/Soltherm.xpt) and are based on the data by Haas et al. (1995) except for sulfate complexes (Migdisov and Williams-Jones, 2008) and halide complexes (Migdisov et al., 2009). See Fowler et al. (2019) for additional information about the database. The REE speciation of the sampled fluids was used to define the initial state in reaction path models, in which exposure of the alkaline spring water to air was simulated by sliding the CO_2 fugacities from $<10^{-10}$ bar to $4*10^{-4}$ bar. The final fCO_2 corresponds to 1.42 mmol DIC kg^{-1}.

4. Results

4.1. Petrography and mineralogy

Baños del Puerto carbonates consist of alternating calcite bands featuring different crystal sizes (Fig. 2D). Some of these bands are composed of large, non-equant, blocky calcite crystals that measure up to 400 µm in diameter (Fig. 2D and E). The second type of calcite band exhibits smaller crystals of darker brownish to yellowish color. BP carbonate samples are predominantly calcite, with minor amounts of quartz, aragonite, and in some cases, dolomite. The Baños del Duque (BD) precipitates are composed almost entirely of large blocky calcite crystals forming irregular bands (Fig. 2F). These carbonates exhibit large void space between the cement bands with porosities as high as 30%. BD carbonate crusts are mostly composed of calcite, and feature accessory quartz, chlorite and chrysotile.

4.2. Hydrochemistry of spring waters

The hyperalkaline spring waters from BD, FR, and FA show high pH values between 11.53 and 11.84, and low concentrations of Mg, nitrate, and DIC compared to the waters from the FB spring (Table 1). Spring waters from FB are characterized by circumneutral pH of 7.45, higher DIC content, higher concentrations in dissolved oxygen and dissolved organic carbon, Ca, Mg, Si, fluoride (F), and nitrate, yet lower concentrations of Na, K, and Cl compared to BD spring waters (Table 1). Only sulfate shows similar values in the four springs, as well as similar Ca

Table 3
Major and trace element contents of travertine carbonates from Baños del Duque and Baños del Puerto. All values in mg kg^{-1}, b.d.l. = below detection limit.

	Mg	Al	Si	Ca	Sc	Ti	V	Cr	Mn	Fe	Co	Ni	Cu	Zn	Sr	Mo	Ba	Sb	As	U	Mg/Sr
Baños del Puerto travertine	2561	814	2893	381500	0.223	16.8	1.38	6.02	16.8	1326	0.818	18.1	1.22	2.97	2603	0.030	106	0.047	1.38	2.06	0.984
	2984	1665	4213	381500	0.269	21.6	1.84	5.33	20.3	2101	1.45	27.6	2.23	2.85	2723	0.012	109	0.127	3.51	2.42	1.10
	5170	1215	3163	381500	0.276	20.8	1.87	13.8	21.6	1058	1.45	50.1	1.06	3.20	2152	0.005	98.1	0.117	0.99	2.14	2.40
	1332	212	1349	381500	0.066	5.97	0.539	3.05	7.24	519	0.395	8.52	1.63	2.82	2905	0.022	141	0.066	0.90	2.65	0.459
	2264	454	3093	381500	0.162	9.00	0.769	6.03	46.3	870	1.07	19.2	1.60	1.53	2801	0.033	112	0.006	1.04	2.39	0.808
	1981	310	2442	381500	0.078	5.21	0.481	4.43	28.8	595	0.808	14.5	1.06	1.35	2763	0.059	108	0.024	0.96	2.54	0.717
	3079	425	3343	381500	0.136	12.8	0.585	4.81	25.8	757	0.976	17.8	1.55	1.68	2622	b.d.l.	107	0.036	1.15	2.51	1.17
Baños del Duque travertine	110	12.7	559	384900	b.d.l.	0.665	0.004	1.27	3.65	80.3	0.019	0.280	0.367	2.17	654	b.d.l.	25.2	0.052	0.147	0.006	0.169
	50	13.6	687	384900	0.092	0.155	0.027	1.31	3.37	70.7	0.035	1.15	0.390	1.72	575	0.006	20.1	0.041	0.291	0.005	0.088
	93	77.1	1000	384900	0.035	0.687	0.141	1.61	3.87	101	0.105	0.92	0.827	2.80	781	0.035	27.3	0.109	0.059	0.015	0.119
	518	166	7360	384900	0.113	3.56	0.215	1.70	3.52	120	0.071	0.005	0.859	1.65	664	0.072	24.3	b.d.l.	0.122	0.015	0.779
	187	239	1052	384900	0.034	4.71	0.384	2.63	5.70	304	0.101	1.98	0.743	2.55	694	0.019	32.4	0.086	0.227	0.019	0.269
	225	627	1546	384900	0.228	26.36	1.56	5.09	23.9	1062	1.79	11.8	1.29	2.26	707	b.d.l.	22.7	0.092	0.368	0.007	0.318
	207	157	1936	384900	b.d.l.	5.28	0.280	4.68	9.92	290	0.442	6.07	1.87	3.18	642	0.111	23.1	0.297	0.195	0.003	0.322
	141	117	1046	384900	b.d.l.	2.28	0.326	3.89	7.70	247	0.243	5.90	1.25	1.77	563	b.d.l.	19.8	0.178	0.061	0.009	0.250
	220	283	1146	384900	0.139	6.13	0.488	2.48	10.5	334	0.647	11.6	1.03	2.72	499	b.d.l.	18.8	0.077	0.150	0.014	0.442
	191	700	2593	384900	0.269	23.7	1.12	3.11	9.39	629	0.462	3.25	1.30	3.29	609	0.109	26.9	0.016	b.d.l.	0.021	0.314
	589	408	1373	384900	0.314	15.7	1.34	26.49	8.04	313	0.476	12.2	1.63	2.24	614	b.d.l.	18.3	0.017	0.090	0.002	0.960
	82.3	89.0	4673	384900	0.274	0.701	0.907	7.04	6.11	181	0.170	b.d.l.	6.81	7.33	756	0.108	15.9	b.d.l.	0.248	b.d.l.	0.109
	170	65.6	3537	384900	b.d.l.	b.d.l.	0.187	7.62	5.15	95.6	0.054	0.964	3.59	7.64	909	b.d.l.	27.1	0.400	0.234	0.007	0.187
	98.1	65.2	1446	384900	b.d.l.	1.07	0.214	2.18	3.66	611	0.142	0.792	1.34	3.37	544	b.d.l.	16.8	0.081	0.023	0.002	0.180
	100	50	1981	384900	b.d.l.	b.d.l.	0.619	9.06	5.17	100	0.132	b.d.l.	5.11	8.04	305	b.d.l.	9.52	0.401	0.632	b.d.l.	0.328

Table 4
Rare earth element contents of travertine carbonates from Baños del Duque and Baños del Puerto. All values in mg kg^{-1}, except Y/Ho, b.d.l. = below detection limit.

	La	Ce	Pr	Nd	Sm	Eu	Gd	Tb	Dy	Y	Ho	Er	Tm	Yb	Lu	∑REE+Y	Y/Ho
Baños del Puerto travertine	0.666	0.838	0.188	0.777	0.186	0.095	0.227	0.028	0.218	1.23	0.036	0.104	0.010	0.079	0.011	4.70	34.5
	0.699	0.790	0.204	0.813	0.212	0.099	0.269	0.032	0.228	1.25	0.044	0.128	0.015	0.087	0.017	4.89	28.4
	0.279	0.456	0.073	0.269	0.094	0.033	0.108	0.024	0.145	1.00	0.040	0.104	0.019	0.052	0.013	2.71	25.0
	0.276	0.263	0.087	0.408	0.138	0.052	0.152	0.030	0.177	1.19	0.036	0.147	0.021	0.093	0.013	3.09	33.5
	0.998	1.01	0.254	1.10	0.344	0.121	0.261	0.038	0.199	1.06	0.046	0.119	b.d.l.	0.063	0.010	5.63	23.3
	0.914	0.870	0.236	1.11	0.232	0.115	0.211	0.028	0.186	0.960	0.037	0.096	0.014	0.061	0.016	5.09	26.0
	0.931	0.866	0.236	0.997	0.280	0.115	0.272	0.044	0.205	0.987	0.031	0.100	0.008	0.077	0.011	5.16	31.5
Baños del Duque travertine	0.018	0.021	0.010	0.019	0.012	b.d.l.	0.007	b.d.l.	b.d.l.	0.031	b.d.l.	0.013	b.d.l.	b.d.l.	b.d.l.	0.130	n.d.
	0.022	0.031	0.007	0.024	0.018	b.d.l.	0.017	b.d.l.	0.004	0.019	b.d.l.	b.d.l.	0.003	b.d.l.	b.d.l.	0.143	n.d.
	0.039	0.046	b.d.l.	0.035	0.026	b.d.l.	b.d.l.	b.d.l.	0.012	0.027	0.007	b.d.l.	b.d.l.	0.009	0.004	0.204	3.73
	0.063	0.140	0.028	0.055	0.012	0.006	0.041	0.004	b.d.l.	0.105	0.012	0.003	0.005	0.021	0.004	0.500	8.57
	0.102	0.195	0.029	0.078	0.020	b.d.l.	0.017	b.d.l.	0.033	0.113	0.002	0.012	0.009	b.d.l.	b.d.l.	0.611	51.8
	0.098	0.186	0.018	0.106	0.143	0.046	0.019	0.006	0.032	0.139	0.005	0.025	0.003	0.022	0.002	0.849	27.6
	0.037	0.053	0.010	0.091	b.d.l.	b.d.l.	0.031	b.d.l.	0.027	0.089	0.007	b.d.l.	0.004	b.d.l.	b.d.l.	0.349	12.8
	0.023	0.067	b.d.l.	0.066	b.d.l.	b.d.l.	0.008	b.d.l.	0.002	0.061	0.008	0.007	0.005	b.d.l.	b.d.l.	0.248	7.49
	0.037	0.067	0.003	0.064	b.d.l.	0.018	0.034	0.004	0.049	0.085	0.007	b.d.l.	b.d.l.	b.d.l.	0.01	0.374	11.8
	0.648	1.361	0.084	0.224	0.110	0.008	0.026	0.019	0.087	0.173	0.017	0.020	0.001	0.006	0.003	2.79	10.3
	0.033	0.097	0.016	0.071	0.043	0.024	0.054	0.009	0.017	0.067	0.002	0.029	b.d.l.	b.d.l.	0.01	0.476	32.2
	0.069	0.069	0.007	b.d.l.	b.d.l.	b.d.l.	b.d.l.	b.d.l.	b.d.l.	0.040	b.d.l.	b.d.l.	b.d.l.	b.d.l.	b.d.l.	0.185	n.d.
	0.366	0.056	0.051	b.d.l.	b.d.l.	b.d.l.	b.d.l.	b.d.l.	0.022	0.130	0.002	0.034	0.004	b.d.l.	b.d.l.	0.665	60.5
	0.037	0.054	0.009	0.065	b.d.l.	0.007	b.d.l.	b.d.l.	b.d.l.	0.030	b.d.l.	b.d.l.	0.002	b.d.l.	b.d.l.	0.205	n.d.
	0.020	0.074	b.d.l.	0.009	0.079	b.d.l.	b.d.l.	0.009	b.d.l.	b.d.l.	0.005	b.d.l.	0.008	b.d.l.	b.d.l.	0.204	n.d.

concentrations in FA and FB springs. Hyperalkaline spring waters from BD, FR, and FA springs have total REE and Y concentrations (∑REE + Y) between 75.4 and 103 ng kg^{-1}, whereas ∑REE + Y concentrations from FB are lower, averaging at 39.0 ng kg^{-1} (Table 2). These higher ∑REE + Y values of the hyperalkaline spring waters are due to the notably higher concentrations of La and Ce compared to the FB waters (Table 2). The enrichment in LREE is prominent in shale-normalized patterns showing elevated La and Ce values in all three hyperalkaline springs and flat shale-normalized REE patterns of the FB waters (Fig. 3). The reported pH and concentrations of main dissolved constituents DIC, Ca, Mg, Na, K, Cl, and Si of the Ronda hyperalkaline fluids are within a similar range as those reported for hyperalkaline spring waters associated with onshore low-temperature serpentinization from Othrys, Argolida, Samail, Troodos, and the Ligurian ophiolites, although particularly the cations show variations among these sites which are not uncommon (Neal and Shand, 2002; Chavagnac et al., 2013b; D'Alessandro et al., 2018; Giampouras et al., 2019; Li Vigni et al., 2021).

4.3. Trace and rare earth element geochemistry of carbonates

Many of the trace element contents in carbonates from BD and BP springs are just above detection limit; one sample from each site was chosen for this study. Rare earth element contents from BD carbonates were mostly below the detection limit, and only the REE contents in carbonate from BP was therefore considered. Trace and REE contents of BD carbonate show a higher spread in most elements except Mg, Sr, U, and Ba compared to carbonate from BP, which exhibits higher contents in all major and trace elements except Si, Cu, and Sb (Figs. 4 and 5, Tables 3 and 4). Trace elements in BD samples exhibit good correlation between Fe and Mn ($r = 0.81$, Fig. 4C), as well as slightly weaker correlations between Al and Ti with the ∑REE + Y ($r = 0.78$ and $r = 0.73$, respectively, Fig. 5B, F), and moderate correlation between U and Ba ($r = 0.63$, Fig. 4D). Moderate correlation of major and trace elements in BP carbonate exists only between Co and Cr ($r = 0.67$), as well as a negative correlation between Mg and Sr ($r = -0.96$, Fig. 4B, E). Shale-normalized REE patterns of BP carbonates reveal negative Ce anomalies, slight positive Eu anomalies, as well as a slight enrichment in HREEs over LREEs (Fig. 6A). Normalizing the REE content of BP carbonate to hyperalkaline fluids from BD reveals a strong fractionation between fluids and carbonates in the LREEs, in particular for La and Ce (Fig. 6B).

4.4. Geochemical modeling

The geochemical reaction path model simulates how the BD hyperalkaline spring water composition changes as it gradually equilibrates with atmospheric CO_2 after discharge. Increasing uptake of atmospheric CO_2 is predicted to cause a decrease in pH from initially 11.5 to 8.4 at the end of the simulation. The simulation indicates that calcite should form from a range of fluid compositions throughout much of the path of titrating in atmospheric CO_2 (Fig. 7A). Along that path, DIC in the fluid is expected to increase from an initial value of 0.03 mmol L^{-1} to 1.45 mmol L^{-1}, while the concentration of dissolved Ca^{2+} decreases from 2.6 mmol L^{-1} to 0.5 mmol L^{-1} due to carbonate precipitation (Fig. 7B). Because the fluids have low sulfate and chloride concentrations, the pronounced changes in pH and DIC in the system are expected to affect the REE speciation such that hydroxide and carbonate REE complexes control the speciation to variable extents. To examine this further, we chose La, Nd, and Lu as representatives for the LREEs, MREEs, and HREEs, respectively, because they show a relatively conservative behavior in low-temperature natural waters as opposed to other REEs that are either redox-sensitive or show fractionation due to adsorption such as Gd, Tb, Ce and Eu (Zhang and Nozaki, 1998; Alibo and Nozaki, 1999). For all REEs, the species distribution changes from a strong dominance of hydroxide species in the hyperalkaline spring fluids toward an increasing role of carbonate speciation with ongoing equilibration with atmospheric CO_2 (Fig. 8A, B, C). For the LREEs, the dominance of $REE(CO_3)_2^-$, $REE(CO_3)^+$, and $REE(HCO_3)^{2+}$ species comes at the expense of the $REEO^+$, $REEOH^{2+}$, $REE(OH)_3$ and $REE(OH)_4^-$ species (Fig. 8A). Before calcite precipitation is predicted to cease (at around $fCO_2 = 10^{-7}$), about half of the dissolved La is expected to be carbonate complexed. The fCO_2 required for carbonate complexation to dominate the MREEs (represented by Nd) is considerably higher, and for the HREEs such as Lu fCO_2 close to air saturation ($fCO_2 = 10^{-4}$) is required to have carbonate speciation take over hydroxo speciation (Fig. 8B and C). Additionally, the REE^{3+} species also increase in concentration with ongoing equilibration with atmospheric CO_2 (Fig. 8A, B, C). Other REE species including sulfate, fluoride, and chloride complexes increase in concentrations along the modeled reaction path (Fig. 8D, E, F). Additionally, there is a change in the distribution among these species from the LREEs to the HREEs. The most abundant sulfate, fluoride, and chloride species for the LREEs are $REESO_4^+$, $REEF^{2+}$, $REECl^{2+}$ and $REE(SO_4)^{2-}$ (Fig. 8D), whereas for the MREEs and the HREEs these are $REESO_4^+$, $REEF^{2+}$, $REECl^{2+}$ and $REEF_2^+$ (Fig. 8E and F). These complexes are overall of minor abundance relative to the

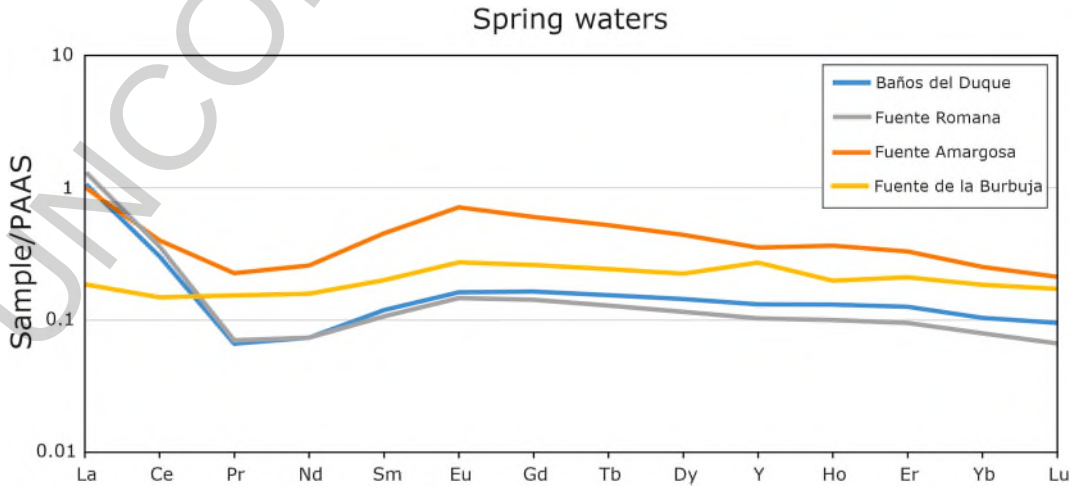

Fig. 3. Shale-normalized rare earth element patterns of hyperalkaline spring waters from Baños del Duque, Fuente Romana, and Fuente Amargosa, and of circumneutral spring water from Fuente de la Burbuja. Different colors refer to the individual samples. PAAS = Post Archean Australian Shale. (For interpretation of the references to color in this figure legend, the reader is referred to the Web version of this article.)

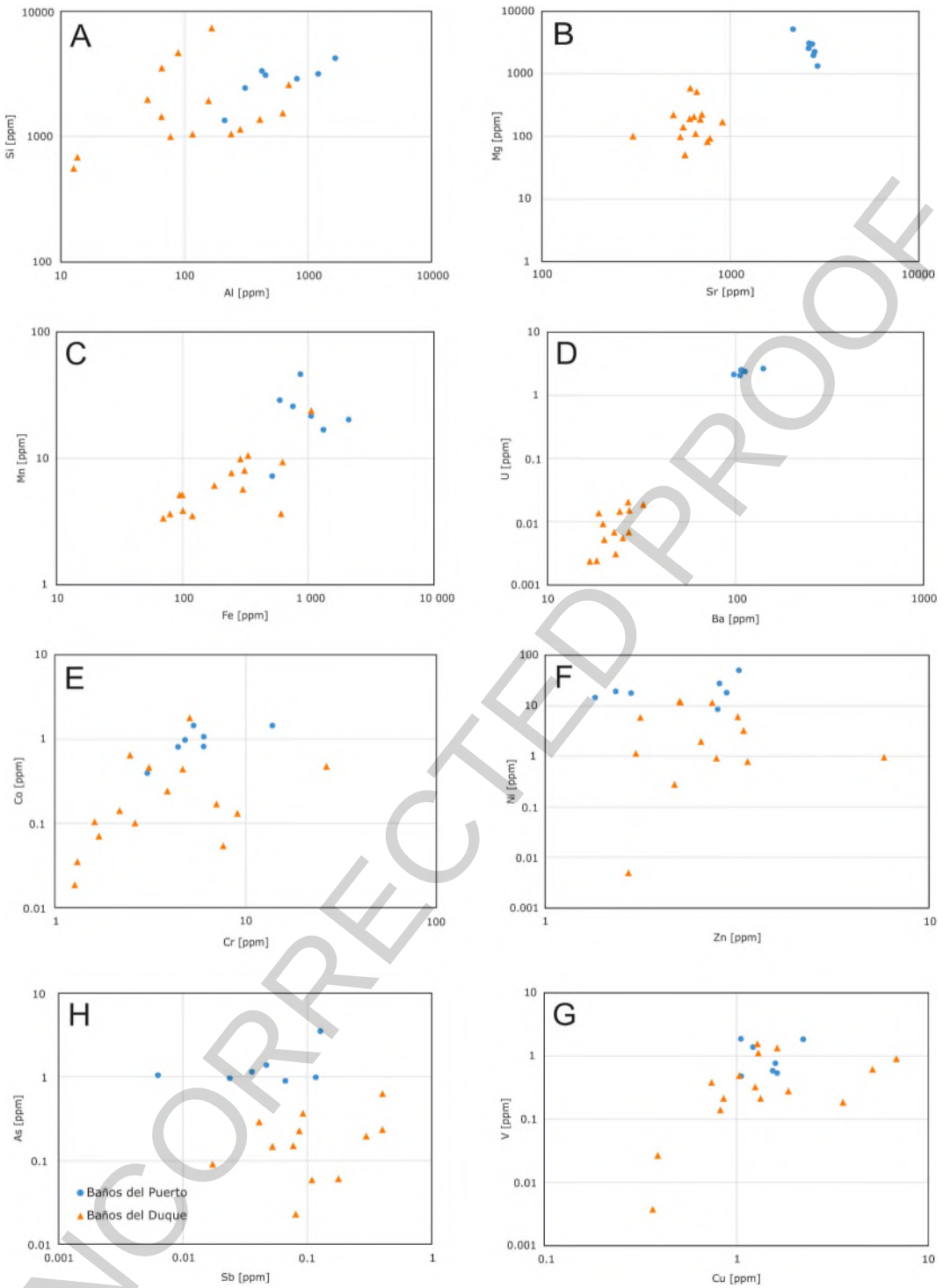

Fig. 4. Distribution of major and trace elements in Baños del Duque and Baños del Puerto travertine carbonates.

hydroxide and carbonate complexes.

Rare earth element species distribution varies between BD and FB spring water samples. Hydroxide REE species dominate spring waters at BD, followed by carbonate, sulfate, fluoride, and chloride species (Fig. 9A). The hydroxide complexes across the REE series are evenly distributed except for La. In contrast, the carbonate, sulfate, fluoride, and chloride species show a stronger preference to complex LREEs compared to the MREEs or the HREEs (Fig. 9A). In FB spring waters, carbonate REE species are most abundant followed by fluoride, hydroxide, sulfate, and chloride species (Fig. 9B). Except for La and Ce, the carbonate complexes show a slight trend towards the HREEs across the REE series. The fluoride, hydroxide, sulfate, and chloride species distribution follows a similar complexation trend as the BD spring waters, decreasing from LREEs to HREEs yet less well developed (Fig. 9B).

The distribution of REE species from the discharging BD hyperalkaline spring water is illustrated in Fig. 10. With the measured composition of the fluid at pH 11.5 and a calculated DIC concentration of 0.028 mmolesL^{-1}, almost all REEs are present in the form of either $REE(OH)_4^-$ or $REE(OH)_3$ complexes (Fig. 10A). Over 90% of dissolved La and Ce is present as $La(OH)_3$ and $Ce(OH)_3$, while most MREEs and HREEs are

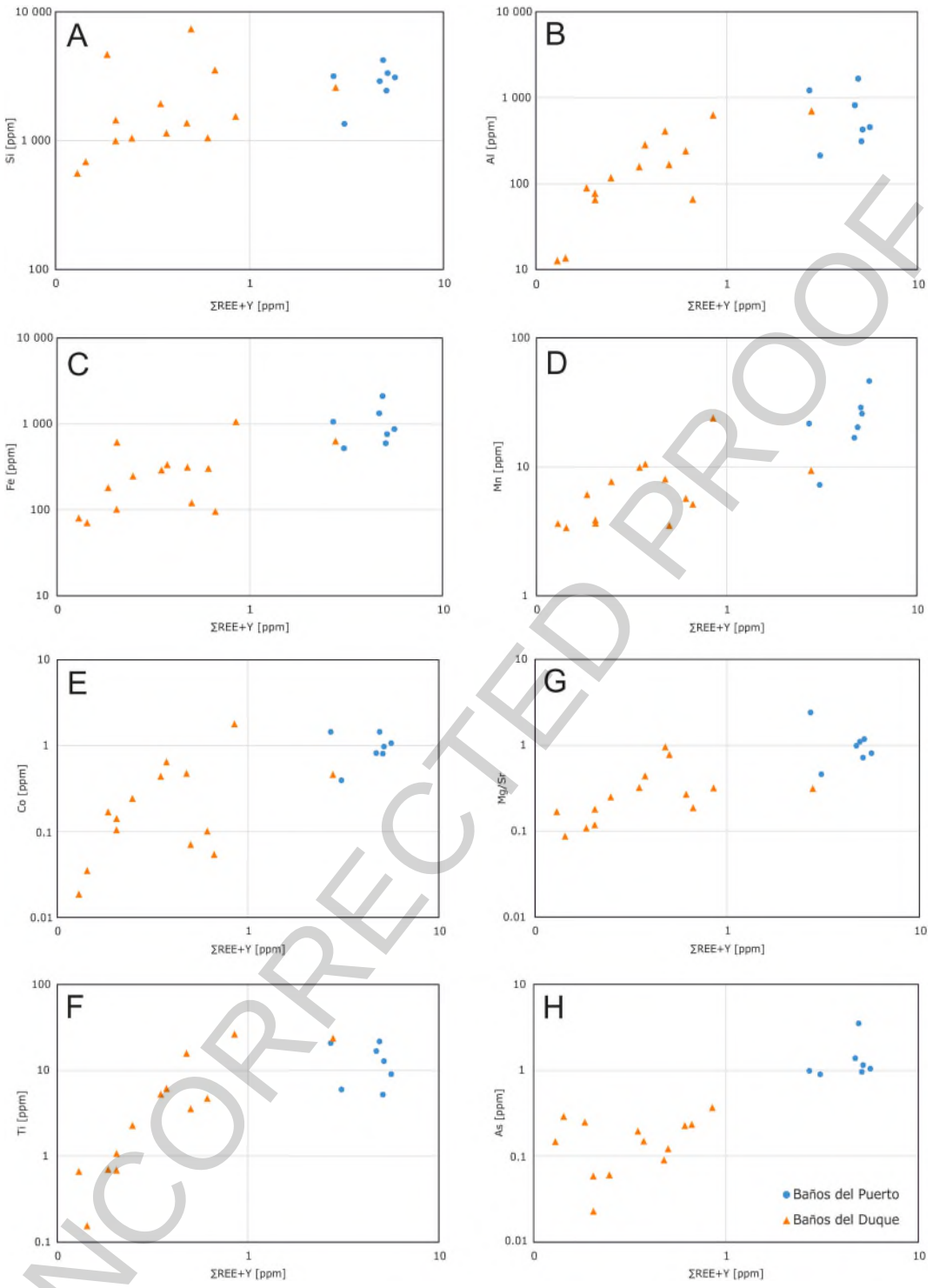

Fig. 5. Distribution of trace and rare earth elements in Baños del Duque and Baños del Puerto travertine carbonates.

almost entirely complexed as $REE(OH)_4^-$ (Fig. 10A). Most other complexes are present in negligible concentrations, whereby $REEO^+$ is most common (Fig. 10B). Modeling of uptake of atmospheric CO_2 by the discharging hyperalkaline fluid shows that REE species distribution changes from the initial very low DIC fluid. A fluid with an fCO_2 of 10^{-7} is half-way between the initial solution and equilibration with the atmosphere, with a calculated pH of 10.4 and a DIC concentration of 0.156 $mmolesL^{-1}$ (Fig. 10C and D). The LREEs are variably complexed as $REE(OH)_3$, $REE(OH)_4^-$, $REEO^+$, $REE(CO_3)_2^-$, and $REECO_3^+$ (Fig. 10C and D). The REE^{3+} and $REE(HCO_3)^{2+}$ complexes are less abundant by comparison (Fig. 10D). At equilibrium with atmospheric CO_2, a pH of 8.3, and a DIC concentration of 1.45 $mmolesL^{-1}$ the two carbonate complexes $REE(CO_3)_2^-$ and $REECO_3^+$ take over REE species distribution, whereby the former is more dominant for all REEs except La (Fig. 10E). Most other REE complexes are negligible at these solution compositions, falling below 1% of the sum of species across the entire REE series (Fig. 10F). To summarize, hyperalkaline spring discharge and following equilibration with CO_2 may cause a rapid switch of REE complexes from mostly hydroxide complexes toward carbonate complexes, yet there are significant differences in complexation among the LREEs, MREEs, and

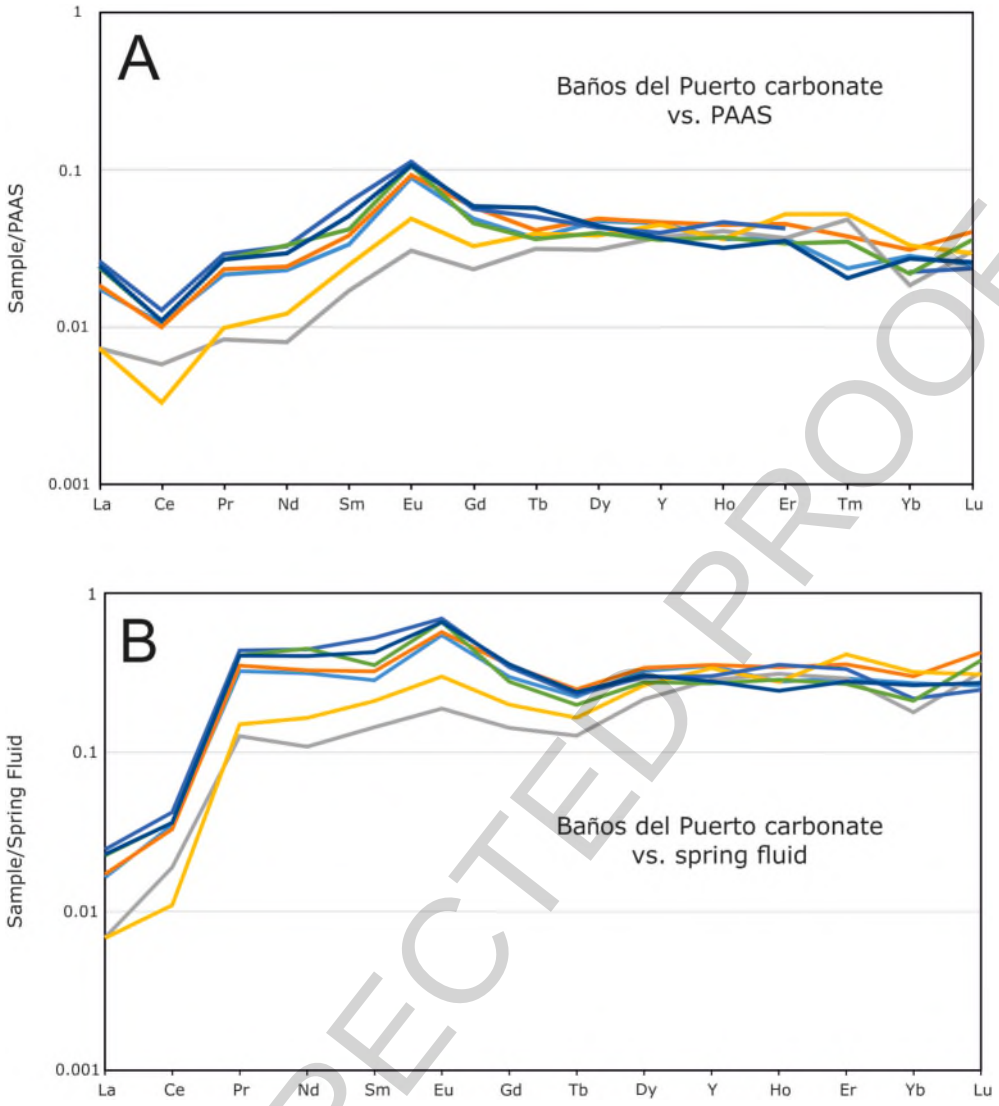

Fig. 6. (A) Shale-normalized rare earth element pattern of travertine carbonate from Baños del Puerto. (B) Fluid-normalized rare earth element pattern of travertine carbonate from Baños del Puerto normalized to hyperalkaline fluids from Baños del Duque. PAAS = Post Archean Australian Shale.

HREEs.

5. Discussion

5.1. REE – hydroxide and carbonate speciation in hyperalkaline fluids

All of the three analyzed hyperalkaline spring waters in the Ronda peridotite show similar REE concentrations and patterns (Table 2, Fig. 3). The BD spring is considered to be representative of the REE chemistry of the hyperalkaline spring water and is used for comparison with the REE concentrations in circumneutral spring waters from the FB spring. Compositional differences between the BD and FB spring waters are reflected in the distribution of dissolved REEs, showing that particularly La and Ce are strongly enriched in the hyperalkaline waters (Table 2, Fig. 3). A possible explanation for the REE distribution in hyperalkaline spring water is selective leaching of the LREEs from the host rocks during subsurface circulation, together with conditions that preserve an aqueous speciation that keeps dissolved forms of REEs in the pore solutions.

Hydroxide and carbonate complexes dominate REE speciation depending on carbon content and pH in alkaline waters (Haas et al., 1995), yet most studies have investigated systems with both high pH and high DIC concentrations (Möller and Bau, 1993; Johannesson et al., 1994b; Pourret et al., 2008). The high pH and low DIC of the Ronda hyperalkaline spring water produces an unusual REE distribution in these fluids, illustrated by the speciation calculations. Due to the low DIC content in BD water, the dominant REE-complexes in hyperalkaline springs are hydroxide complexes (Fig. 9A). Speciation modeling of hyperalkaline spring water reveals a strong fractionation in speciation between the REE series, where La and Ce are dominantly present as $REE(OH)_3$, and all MREEs and HREEs are present as $REE(OH)_4^-$ complexes (Fig. 10A). Is it a coincidence that La and Ce are the only REEs enriched in the hyperalkaline spring waters? The REE contents of calcite shows that La and Ce are discriminated against the other REEs during incorporation by the precipitating calcite (cf. Fig. 6B). During crystallization of calcite, which is predicted to take place primarily between pH 11.5 and 10.5 (and $fCO_2 < 10^{-9}$), the speciation of REEs is expected to remain principally controlled by the two hydroxide complexes (cf. Fig. 10a and c): La and Ce are the two REEs that are initially dominated by complexation as neutral $REE(OH)_3$ complexes; the other REEs form chiefly $REE(OH)_4^-$ complexes. Perhaps the negatively charged MREE and HREE complexes are preferentially incorporated in the growing calcite crystals. If correct, calcite precipitation could be responsible for the REE pattern shape of the hyperalkaline waters.

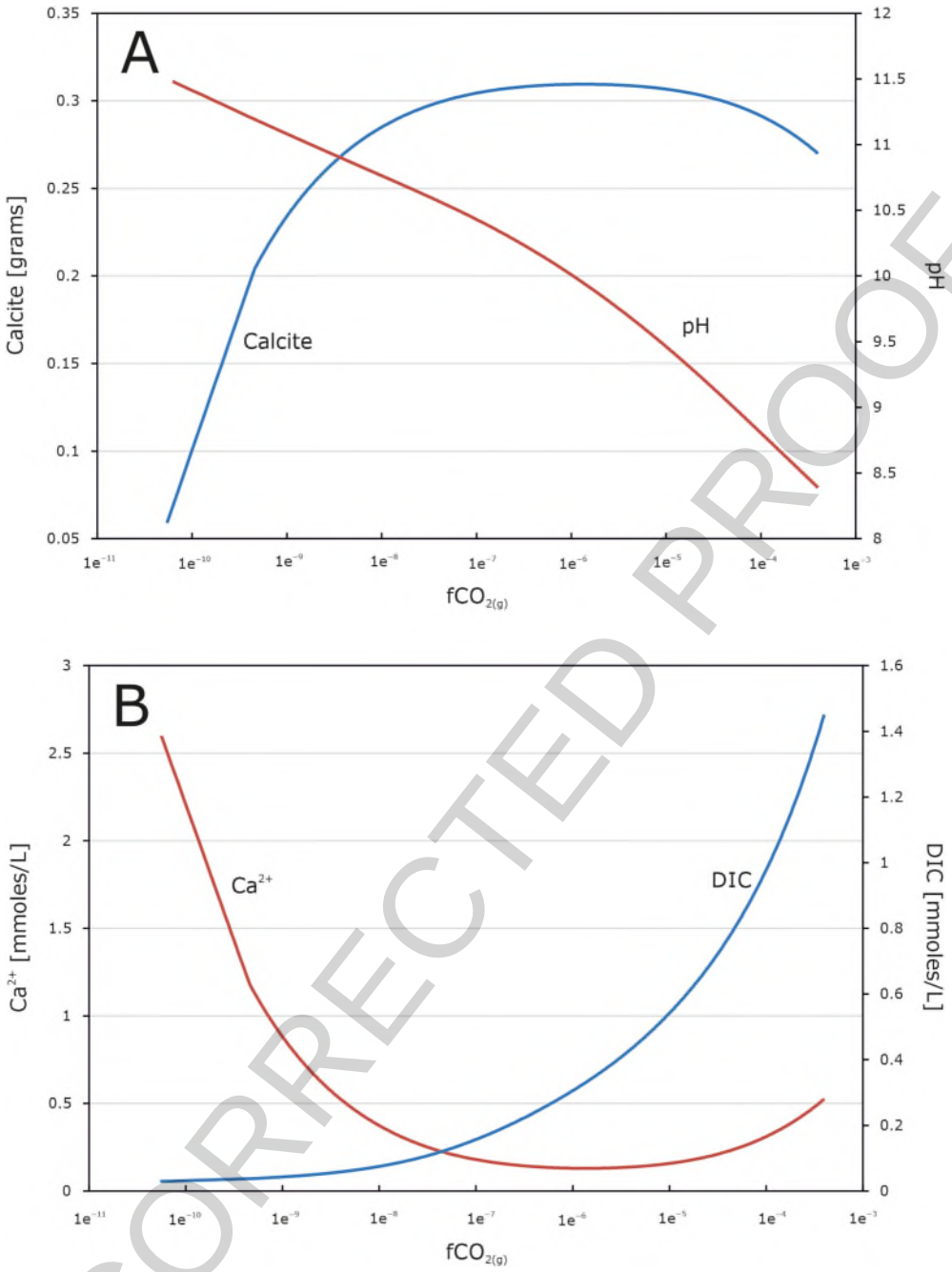

Fig. 7. Results of reaction path modeling. (A) Precipitation of calcite and evolution of Baños del Duque hyperalkaline fluid pH during equilibration with atmospheric CO_2. (B) Evolution of dissolved calcium (Ca^{2+}) and dissolved inorganic carbon (DIC) in Baños del Duque hyperalkaline spring fluids during equilibration with atmospheric CO_2. See text for details.

In FB waters, REE complexation is governed by the much higher concentrations in DIC, resulting in a dominance of carbonate complexes, specifically for the MREEs and HREEs (Fig. 9B). This difference in REE complexation behavior is further represented by geochemical modeling of chemical water evolution during emission of hyperalkaline fluids from the springs, and their stepwise equilibration with atmospheric CO_2. Diffusion of gaseous CO_2 into discharging high-Ca, low-DIC, type II fluids is fast and effective in onshore low-temperature serpentinization systems where it is kinetically controlled by CO_2 hydroxylation (Clark and Fontes, 1990; Clark et al., 1992). This rapid uptake of carbon not only triggers carbonate precipitation (Neal and Stanger, 1985; Clark and Fontes, 1990; Paukert et al., 2012), but also causes a shift in the distribution of REE complexes in solution. This speciation shift varies across the REE-series as illustrated in Fig. 8. Although there is a general shift from hydroxide to carbonate REE complexes, the sensitivity of this shift toward DIC concentrations is particularly strong for the LREEs, whose hydroxide complexes are dominant in the initial hyperalkaline fluid, while becoming negligible at equilibrium with atmospheric CO_2 partial pressure (Fig. 8A). For the MREEs such as Nd this speciation shift requires more CO_2 uptake into the fluid (Fig. 8B), and even more CO_2 uptake for the HREEs such as Lu (Fig. 8C). In the pH range around and above 10, solution pH has a stronger effect on speciation with dominating hydroxide complexes (Fig. 10C), whereas with increasing DIC content above approximately 0.15 mmol L^{-1}, speciation is more strongly controlled by carbon content (Fig. 10E). The tipping point where carbon content begins to control REE speciation varies across the REE series,

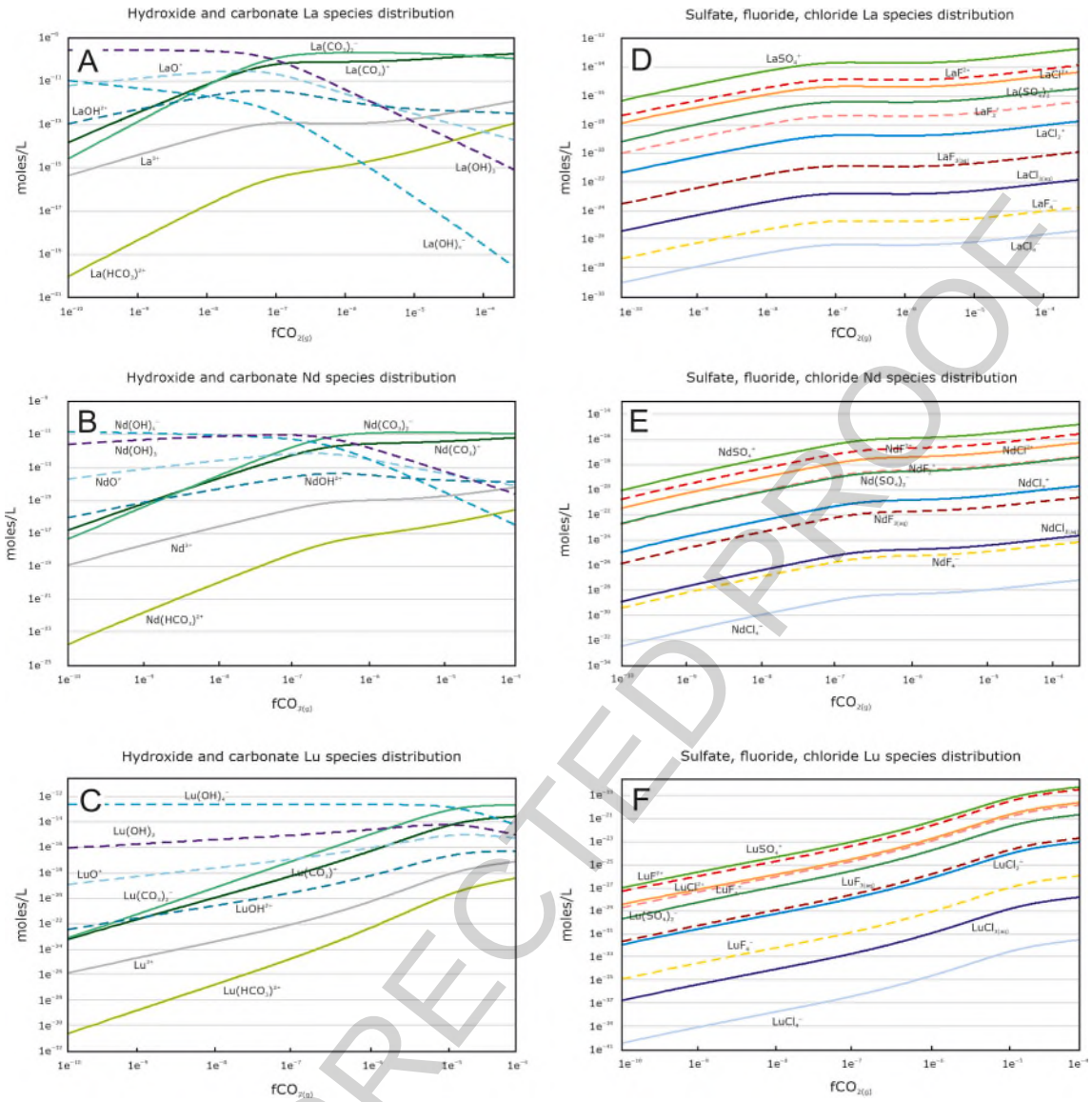

Fig. 8. Reaction path modeling results showing the evolution of rare earth element speciation of hyperalkaline spring fluids during equilibration with atmospheric CO_2. See text for details.

with higher DIC contents required for the MREEs and HREEs than for the LREEs (cf. Fig. 8A, B, C). This observation is due to three main effects, (1) the strong hydroxide complexation of the MREEs and LREEs, (Fig. 8B and C, 10A, B), (2) the strong hydroxide complexation of the LREEs particularly La, Ce, and to a lesser extent Pr (Figs. 8A and 10 A, B), and (3) the general dominance of carbonate complexes beyond a $pCO_2 = 1*10^{-6}$, which equates to a pH of 10 and DIC concentrations between 0.2 and 0.3 mmol L^{-1} (Fig. 7). This is an unusual complexation behavior for terrestrial freshwater environments, where hydroxide complexes usually dominate between a pH of 3 and 8 (Schijf and Byrne, 2001). The dominance of hydroxide complexes in the high pH, low DIC hyperalkaline spring fluids is due to their very low carbon content in which carbonate complexes are subordinate (Figs. 9A and 10A, C). It should further be noted that pH drops from an initial value of 11.5 to 10, whereby DIC concentration rises by a factor of 10 from 0.02 to over 0.2 mmol L^{-1} (Fig. 7), suggesting that the changes in REE distribution and complexation during diffusion of atmospheric CO_2 into hyperalkaline fluids are affected to a larger degree by an increase in carbon content than by a decrease in pH.

The distribution of $REE(CO_3)_2^-$ and $REE(CO_3)^+$ species is strongly dependent on pH and on the size of the respective REE. The enrichment of HREEs in seawater, for example, is attributable to the carbonate complex $REE(CO_3)_2^-$ (Cantrell and Byrne, 1987), and similar REE complexation effects by DIC were suggested for the alkaline Mono Lake where REEs are also complexed by $REE(CO_3)_2^-$ (Johannesson and Lyons, 1994a). The two carbonate complexes $REE(CO_3)_2^-$ and $REE(CO_3)^+$ are usually dominant in natural waters (Byrne and Sholkovitz, 1996; Tang and Johannesson, 2003), and their stability depends on the REE atomic number (Luo and Byrne, 2004). This is also shown by the reaction path modeling results of hyperalkaline spring discharge, where $REE(CO_3)_2^-$ and $REE(CO_3)^+$ species make up over 99% of all REE complexes at equilibrium with atmospheric CO_2 (Fig. 10E). Except for La, the REE $(CO_3)_2^-$ complex is slightly more abundant than $REE(CO_3)^+$, such that both complexes occur in a $REE(CO_3)_2^-$: $REE(CO_3)^+$ ratio of 60:40 to almost a 50:50 ratio for the LREEs (Fig. 10E). In seawater, at DIC concentrations of $1.38*10^{-4}$ mol L^{-1}, the $REE(CO_3)_2^-$ species preferentially complexes the HREEs, contributing more strongly to the HREE-enriched shale-normalized pattern than the $REE(CO_3)^+$ complex, which is more dominant for the LREEs under these conditions (Cantrell and Byrne, 1987). The hyperalkaline fluids show a different trend, where the much lower DIC contents of $2.8*10^{-5}$ mol L^{-1} (Fig. 10A) leads to a preferred carbonate complexation to the LREEs across the REE series (Fig. 9A). As

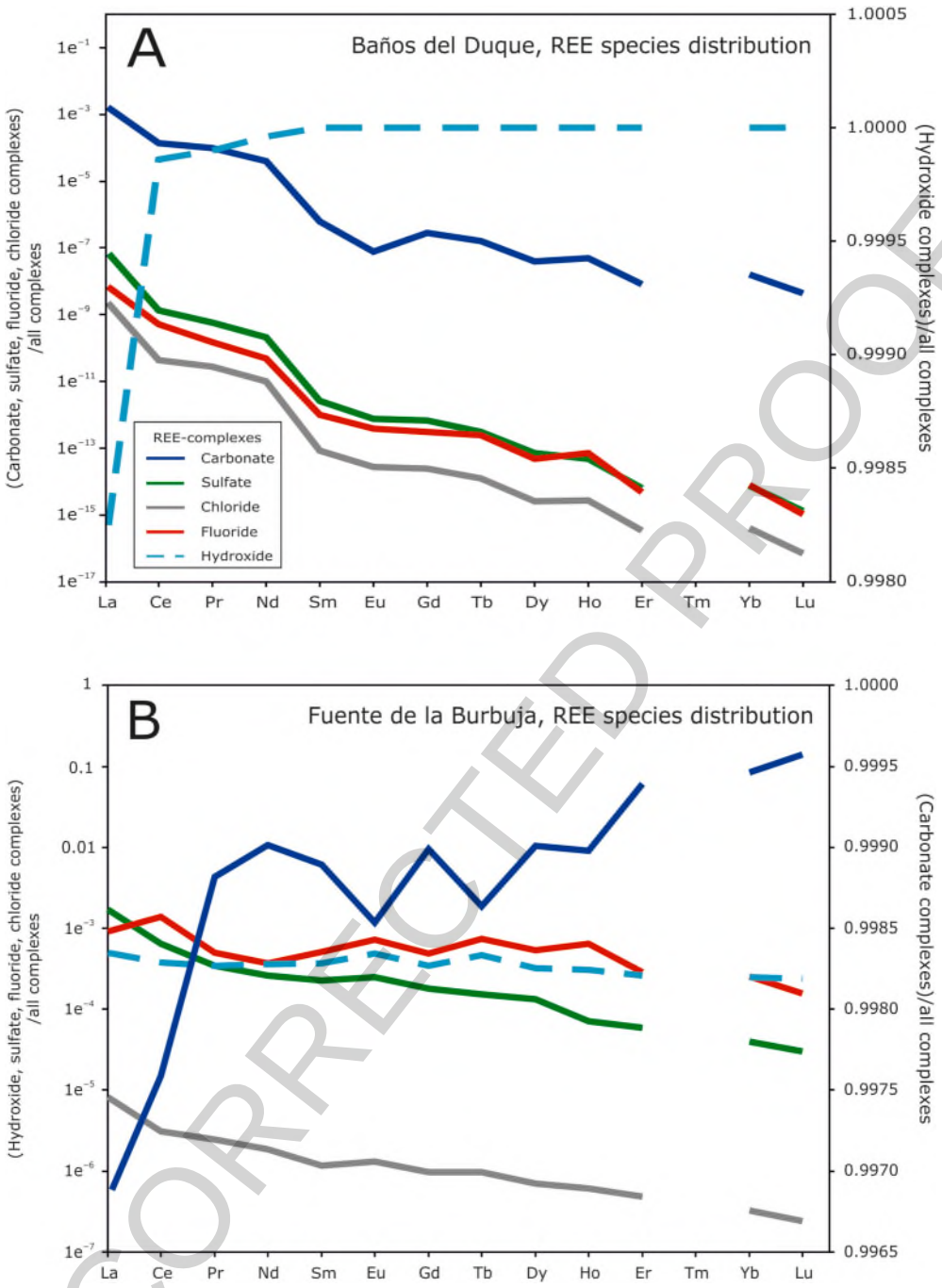

Fig. 9. Rare earth element species distribution in (A) hyperalkaline fluids of Baños del Duque, and (B) circumneutral fluids of Fuente de la Burbuja. See text for details.

the hyperalkaline fluid approaches equilibrium with atmospheric CO_2 reaching DIC concentrations of up to $1.45*10^{-3}$ mol L^{-1} (Fig. 10E), the distribution of $REE(CO_3)_2^-$ and $REE(CO_3)^+$ complexes evolves toward those observed in seawater with the former being preferentially complexed by the HREEs, and the latter by the LREEs (Fig. 10E, cf. Cantrell and Byrne, 1987, their Fig. 2).

5.2. *Subordinate REE complexes in hyperalkaline fluids*

The hyperalkaline spring waters are depleted in almost all major and trace elements compared to the circumneutral waters emitted from the FB spring (Table 1). Exceptions are Na, K, and Cl, which are elevated compared to FB waters, and sulfate, which is present in roughly similar concentrations in all four springs (Table 1). The sulfate, chloride, and fluoride complexes in hyperalkaline water show a stronger preference for the LREEs compared to the MREEs and the HREEs (Fig. 9A), which is not as clearly observable for the circumneutral FB waters (Fig. 9B). This distribution is probably due to a combined effect of pH and DIC content. Chloride complexes with REEs are weak at ambient temperatures (Gammon et al., 1996; Luo and Byrne, 2001), which may explain their comparatively low occurrence despite significant concentrations of chloride in the spring fluids. However, the general trend that LREEs are complexed more readily to chloride than the HREEs (Wood, 1990) is observed for hyperalkaline and circumneutral fluids (Fig. 9), yet to a higher degree for the hyperalkaline fluid. The most common non-hydroxide, non-carbonate REE species is REE^{3+}, which becomes

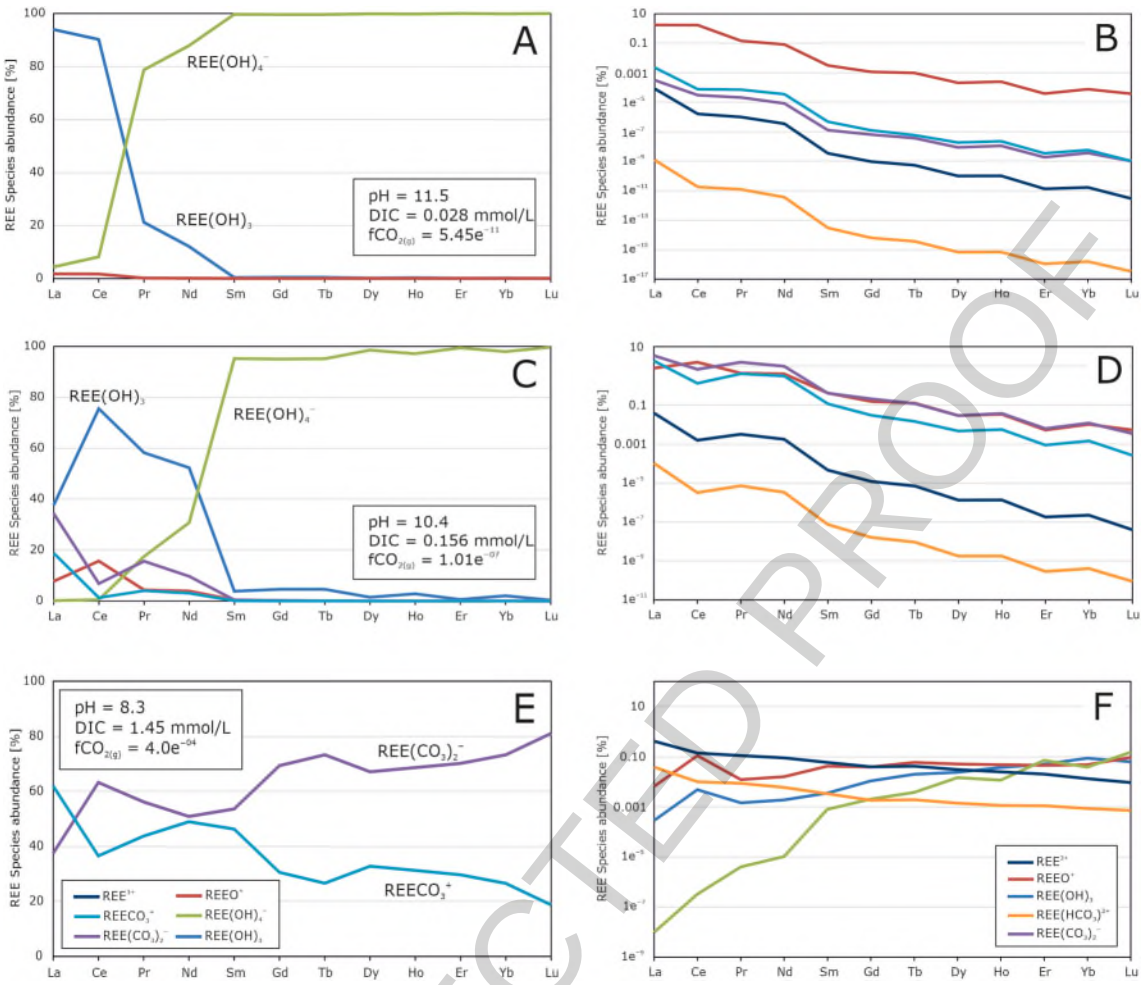

Fig. 10. Abundance of rare earth element species in Baños del Duque hyperalkaline fluids at various stages of the reaction batch modeling during equilibration with atmospheric CO_2. See text for details.

quantitatively more relevant with decreasing pH and increasing DIC concentrations approaching equilibrium with atmospheric CO_2 (Fig. 8A, B, C). The dominance of the REE^{3+} species over chloride complexes may be caused by the ambient temperatures of the hyperalkaline spring fluids, because chloride complexes dominate solutions only at higher temperatures even when Cl concentrations are low (Haas et al., 1995; Migdisov and Williams-Jones, 2008). Although the hyperalkaline spring waters contain little F (Table 1), the $REEF^{2+}$ complex is one of the most common among the subordinate complexes across the REE series (Fig. 8D, E, F). The relative overrepresentation of REE-fluoride complexes despite low F concentrations may be due to the very low stability of hydrofluoric acid. Hydrofluoric acid is a weaker acid than hydrochloric acid, and dissociates to H^+ and F^- at neutral to more alkaline conditions (Bach et al., 2003; Migdisov and Williams-Jones, 2014), providing more F for REE complexation compared to other elements such as Cl in hyperalkaline spring fluids. Even though DIC content in hyperalkaline springs is very low, sulfate concentrations are even lower (Table 1), yet the $REESO_4^+$ complex is the most common among the subordinate complexes (Figs. 8D and 9A). Sulfate complexation with the REEs in terrestrial waters is typically more relevant in acidic groundwater, since circumneutral to alkaline conditions usually favor REE complexation by carbonate species (Tang and Johannesson, 2003). Although it has been suggested that sulfate complexes show little preference between LREE and HREEs (Wood, 1990), they appear to be preferentially complexed by the LREEs in hyperalkaline fluids, similar to the carbonate, chloride, and fluoride complexes (Fig. 9A). In the circumneutral FB spring waters this complexation behavior is less well developed despite similar sulfate concentrations compared to the hyperalkaline spring waters (Fig. 9B, Table 1). As with the distribution of the other complexes, REE-sulfate complexation in hyperalkaline spring water is strongly affected by high pH and low DIC concentration, leading to an unusual complexation behavior compared to other terrestrial waters.

5.3. *Carbonate precipitation and trace element incorporation*

Authigenic carbonates associated with hyperalkaline spring discharge from the Ronda peridotite are predominantly composed of calcite. The presence of lamination and blocky calcite crystals are typical for terrestrial travertine (Flügel, 2004; Claes et al., 2015), and the lack of microbial laminae, overgrowths, crusts, or peloidal, agglutinated, dendrolitic, or stromatolitic fabrics observed in other travertine deposits (Gandin and Capezzuoli, 2014; Claes et al., 2017) agrees with an abiotic precipitation mechanism for the BP and BD carbonates. The absence of botryoidal fans further argues for precipitation in a quiet, non-turbulent flow regime without large terraces with steep, subvertical slopes (Gandin and Capezzuoli, 2014), which is in accord with the observed flow regime and topography at the BD and BP spring sites (Etiope et al., 2016; Giampouras et al., 2019).

Strontium is often present in high contents in aragonite relative to crustal values or other carbonate polymorphs and usually precipitates as travertine at high temperatures (>50 °C), whereas low-Mg calcite in travertine incorporates less Sr and precipitates at ambient temperatures (Guo and Riding, 1992; Fouke et al., 2000). Strontium contents in

carbonates may reflect its concentration in parent fluids (Zhao and Zheng, 2014; Castorina et al., 2020), and Sr substitutes for Ca or Mg at the Ca^{2+} lattice site in travertines (Banner, 1995). The high Sr content in BD carbonates, and even higher contents in BP samples is unusual for calcite travertines associated with cool, hyperalkaline springs waters. High Sr contents in travertines have been reported from travertines precipitating from hydrothermal spring waters, and have been interpreted as being sourced from hydrothermal fluids (Castorina et al., 2020). Both Ba and Sr partition preferably into aragonite due to the nine-fold coordination of the cations in the orthorhombic crystal lattice (Parekh et al., 1977; Reeder et al., 1999). Barium partition coefficients are higher for aragonite than for calcite in hot spring travertines, and Ba loss occurs during aragonite neomorphism to calcite (Sturchio et al., 1998; Teboul et al., 2016). The higher Sr contents in the carbonate at BP is likely due to the presence of minor aragonite, and may be unrelated to Sr concentrations in the spring waters (between 1.8 and 2.4 μmol L^{-1}, Giampouras et al., 2019). Similar mineralogical effects have also been reported for U, which is preferentially incorporated as UO_2^{2+} uranyl ion into the crystal lattice of aragonite (Reeder et al., 2000; Kelly et al., 2003). A mineralogical dependence on the incorporation of Ba, Sr, and U has previously been observed for both hypogean and epigean travertines (Teboul et al., 2016). The presence of aragonite in BP carbonates was also reported by Giampouras et al. (2019), who argued that its precipitation over calcite may have been enabled by seasonal mixing of hyperalkaline spring fluids with circumneutral river water that occurs in close vicinity to the discharging spring site at BP. The high Ba contents in BP travertines are unusual, particularly since Ba concentrations in parent fluids are very low, between 0.02 and 0.03 μmol L^{-1} (Giampouras et al., 2019). Barium contents in BP travertines are higher than those from BD, yet lower than those reported from travertines associated with hyperalkaline springs from the Ligurian ophiolite (Teboul et al., 2016). The sources and variable contents of Ba in BP and BD carbonates cannot be determined at present, yet some of the observed variability may be related to varying contents of Ba-containing minerals weathering to different degrees during subsurface water-rock interactions. Barium, along with Sr and U, partitions preferably into aragonite over calcite (Böttcher and Dietzel, 2010), and the enrichments of these three elements is most likely a function of mineralogy in the case of the Ronda travertine carbonates. The enrichment of most of the analyzed trace elements in BD carbonates over BP carbonates (Figs. 4 and 5) may either be due to the presence of detrital minerals in the travertine, as laser ablation cannot completely avoid contamination by clay minerals interspersed within the carbonate phases (e.g. Zwicker et al., 2018b; Smrzka et al., 2020), or due to different concentrations of these elements in parent fluids. The exact cause of the discrepancies in trace element contents among the two investigated travertine deposits cannot be further assessed at this point, because the concentrations of many of the trace elements in the host rock and in the spring fluids are presently unknown.

5.4. Rare earth element composition of travertines and uptake during precipitation

Rare earth element contents in BP carbonates are at least one order of magnitude higher than those determined for BD carbonates. This distribution does not appear to be a function of low-temperature serpentinization of ultramafic rocks in the subsurface, because REEs in travertines from the BD hyperalkaline springs were mostly too low to obtain coherent shale-normalized REE patterns (Table 4). Some of the REEs in BD carbonates may have been derived from detrital material present within the carbonate crusts as suggested by the slightly positive correlations of ∑REE + Y and Co, Ti, and Al (Fig. 5B, E, F), which are elements typically associated with detrital clay minerals (Nothdurft et al., 2004; Tribovillard et al., 2006; Schier et al., 2021). A contribution of clay minerals to the ∑REE + Y in travertine carbonates is probably minor due to the absence of such correlations in BP carbonates, and the higher ∑REE + Y concentrations in BP carbonates was therefore inherited primarily from the parent fluids.

Total REE contents in BP carbonates show no correlation with any other element (Fig. 5), and show negative Ce and positive Eu anomalies in their PAAS-normalized patterns (Fig. 6A). These two anomalies are not uncommon for travertine carbonates, and have been interpreted as reflecting the composition of the source material from which the springs were emitted (Claes et al., 2019; Castorina et al., 2020). Positive Eu anomalies are likely caused by preferable weathering of Eu-rich minerals in the subsurface (cf. Banks et al., 1999). Oxygenated seawater and freshwater usually exhibit negative Ce anomalies (e.g. Alibo and Nozaki, 1999; Leybourne et al., 2000) due to the removal of Ce^{3+} by oxidation and adsorption of Ce^{4+} onto particulates (Moffett, 1990; Sholkovitz et al., 1994). Dissolved oxygen concentrations in hyperalkaline fluids are low (between ~1.74 and 2.49 mg L^{-1}) compared to the circumneutral spring fluids at 8.89 mg L^{-1} (Table 1), and significantly lower than for seawater or freshwater in equilibrium with the atmosphere (Benson and Krause, 1984). Negative Ce anomalies, which are absent in shale-normalized REE patterns in the spring waters (Fig. 3), as well as the shale-normalized HREE enrichment pattern, confirm that travertine formation occurred from a fluid with a different composition than that of the hyperalkaline fluids in the subsurface. The discrepancy between REE distribution in hyperalkaline fluids and travertine is illustrated best by the large fractionation of La and Ce between the fluid and the solid phase (Fig. 6B). Calcite formation begins quickly after hyperalkaline fluid discharge and CO_2 uptake, reaching a plateau and decreasing again as pCO_2 approaches atmospheric equilibrium (Fig. 7A). Reaction path modeling also shows that calcite precipitation proceeds at a pH above 9.5 (Fig. 7A), beyond the point of zero charge of calcite at 9.5 (Somasundaran and Agar, 1967), which suggests a negatively charged surface with a potential to sorb cations from solution in the early stages of mineral precipitation. Given the differences in REE distribution between the hyperalkaline spring fluid and the travertine, REE uptake into the crystal lattice occurred sometime after fluid emission during later calcite growth as the spring fluids approached equilibrium with the atmosphere. Precipitation at higher DIC and pCO_2 most likely produced the HREE-enriched shale-normalized patterns due to strong complexation of HREEs by carbonate species, similar to HREE-enriched patterns observed for seawater (Cantrell and Byrne, 1987; Byrne and Kim, 1990). The REEs were therefore most likely taken up by the mineral (1) at a pH between 9.5 and 10, (2) at DIC concentrations well above those determined in the initial hyperalkaline spring fluid, (3) at higher dissolved O_2 concentrations than present in the discharging fluids, and (4) at a point where the calcite surface was approaching its point of zero charge. This further suggests that REE sorption onto freshly precipitating calcite crusts in the initial stages of travertine formation does not necessarily lead to their immediate incorporation into the growing crystal. Some degree of fluid-mineral equilibration, as well as ongoing precipitation in a supersaturated solution is required for the REEs to be incorporated into the crystal lattice. Additionally, calcite precipitation ceases at a pH between 9.5 and 10, and at a lower pH (due to the increasing pCO_2) even some dissolution of calcite is expected (Fig. 7A). Dissolution-reprecipitation reactions, such as aragonite transformation to calcite in the case of the BP spring site, may further modify the composition of initially adsorbed trace metals onto the mineral as suggested by enrichments of Ba, Sr, and U. The final REE composition in travertine is reached when precipitation and dissolution reactions in the parent fluid are in equilibrium.

6. Conclusions

This study presents the first detailed investigation of the behavior of dissolved REEs in fluids of hyperalkaline springs associated with onshore, low-temperature serpentinization. Using a comparative approach of trace element geochemistry of fluids and travertine carbonates from several hyperalkaline and circumneutral springs, in

combination with geochemical reaction path modeling, it becomes evident that REE behavior in these setting is largely different from most other terrestrial freshwater environments. The main cause for the observed distribution of REE species in hyperalkaline spring waters is their very high pH combined with a very low concentration in DIC, leading to a particular REE complexation behavior. REE contents in travertine carbonates are not representative of their respective concentrations in the parent fluids. Moreover, ongoing precipitation of travertine shortly after fluid discharge may have a yet unknown partitioning effect between REE distribution in parent fluids and REE content in the solid phase; negatively charged MREE and HREE species are possibly taken up more efficiently by the precipitating calcite than the LREEs. The high contents in travertines compared to hyperalkaline discharging fluids clearly show that the precipitates are major sinks for REEs, but also for other elements such as Sr, Ba, and U in these settings. These first results on trace and rare earth element distributions in authigenic carbonates associated with onshore low-temperature serpentinization may improve their use in future carbon capture, storage, and remediation strategies by providing first-order constraints on their chemical composition, as well as insights into the mechanisms of their uptake by precipitating minerals.

Declaration of competing interest

The authors declare that they have no known competing financial interests or personal relationships that could have appeared to influence the work reported in this paper.

Data availability

Data will be made available on request.

Acknowledgments

Jennifer Zwicker acknowledges financial support from the Austrian Science Fund (FWF grant number T 1189-N). We thank Susanne Gier from the University of Vienna for XRD analysis, as well as Patrick Monien from the University of Bremen for determining trace and rare earth elements in authigenic carbonates. We are grateful to Franziska Klimpel and Andrea Koschinsky from the Jacobs University for measuring the REE and Y concentrations of the spring waters. This is article is also a contribution to the Research Groups RNM-308 and RNM 128 of the “Junta de Andalucía” and the project “Hidrogeoquímica de las Peridotitas de Ronda: Caracterización de las Aguas Subterráneas y del Metano Asociado (UMA18-FEDERJA-101).

References

Abbott, A.N., Haley, B.A., McManus, J., Reimers, C.E., 2015. The sedimentary flux of dissolved rare earth elements to the ocean. Geochem. Cosmochim. Acta 154, 186–200.
Alibo, D.S., Nozaki, Y., 1999. Rare earth elements in seawater: particle association, shale-normalization and Ce oxidation. Geochem. Cosmochim. Acta 63, 363–372.
Bach, W., Roberts, S., Vanko, D.A., Binns, R.A., Yeats, C.J., Craddock, P.R., Humphris, S. E., 2003. Controls of fluid chemistry and complexation on rare-earth element contents of anhydrite from the Pacmanus subseafloor hydrothermal system, Manus Basin, Papua New Guinea. Miner. Deposits 38, 916–935.
Banks, D., Siewers, U., Sletten, R.S., Haldorsen, S., Barrie, D., Heim, M., Swensen, B., 1999. The thermal springs of Bockfjorden, Svalbard: II: selected aspects of trace element hydrochemistry. Geothermics 28, 713–728.
Banner, J.L., 1995. Application of the trace-element and isotope geochemistry of strontium to study of carbonate diagenesis. Sedimentology 42, 805–824.
Barnes, I., O'Neil, J.R., 1971. Calcium-magnesium carbonate solid solutions from Holocene conglomerate cements and travertines in the Coast Range of California. Geochem. Cosmochim. Acta 35, 699–718.
Barnes, I., O'Neil, J.R., 1969. The relationship between fluids in some fresh alpine-type ultramafics and possible modern serpentinization, western Unites States. Geol. Soc. Am. Bull. 80, 1947–1960.
Barnes, I., LaMarche, V.C., Himmelberg, G., 1967. Geochemical evidence of present-day serpentinization. Science 156, 830–832.
Barnes, I., O'Neil, J.R., Trescases, J.J., 1978. Present day serpentinization in New Caledonia, Oman and Yugoslavia. Geochem. Cosmochim. Acta 42, 144–145.
Benson, B.B., Krause, D., 1984. The concentration and isotopic fractionation of oxygen dissolved in freshwater and seawater in equilibrium with the atmosphere. Limnol. Oceanogr. 29, 620–632.
Bethke, C.M., 2005. The Geochemist's Workbench® Release 6.0 (Four Volumes). Hydrogeology Program. University of Illinois, Urbana, Illinois.
Blank, J.G., Green, S.J., Blake, D., Valley, J.W., Kita, N.T., Treiman, A., Dobson, P.F., 2009. An alkaline spring system within the Del Puerto Ophiolite (California, USA): a Mars analog site. Planet. Space Sci. 57, 533–540.
Böttcher, M.E., Dietzel, M., 2010. Metal-ion partitioning during low-temperature precipitation and dissolution of anhydrous carbonates and sulphates. Eur. Mineral Union Notes Mineral 10, 139–187.
Bruni, J., Canepa, M., Chiodini, G., Cioni, R., Cipolli, F., Longinelli, A., Marini, L., Ottonello, G., Vetuschi-Zuccolini, M., 2002. Irreversible water-rock mass transfer accompanying the generation of the neutral, Mg-HCO_3 and high-pH, Ca-OH spring waters of the Genova province. Italy. Appl. Geochem. 17, 455–474.
Byrne, R.H., Kim, K.-H., 1990. Rare earth element scavenging in seawater. Geochem. Cosmochim. Acta 54, 2645–2656.
Byrne, R.H., Sholkovitz, E.R., 1996. Marine chemistry and geochemistry of the lanthanides. In: Bünzli, J.-C.G., Pecharsky, V.K. (Eds.), Handb. Phys. Chem. Rare Earths 23, 497–593.
Cantrell, K.J., Byrne, R.H., 1987. Rare earth element complexation by carbonate ion and oxalate ions. Geochem. Cosmochim. Acta 51, 597–605.
Casanova, J., Bodenan, F., Negrel, P., Azaroual, 1999. Microbial control on the precipitation of modern ferrihydrite and carbonate deposits from the Cézallier hydrothermal springs (Massif Central, France). Sediment. Geol. 126, 125–145.
Castorina, F., Masi, U., Billi, A., 2020. Assessing the origin of Sr and Nd isotopes and (REE+Y) in Middle-Upper Pleistocene travertines from the Acquasanta Terme area (Marche, central Italy) and implications for neotectonics. Appl. Geochem. 117, 104596.
Chavagnac, V., Ceuleneer, G., Monnin, C., Lansac, B., Hoareau, G., Boulart, C., 2013a. Mineralogical assemblages forming at hyperalkaline warm springs hosted on ultramafic rocks: a case study of Oman and Ligurian ophiolites. G-cubed 14. https://doi.org/10.1002/ggge.20146.
Chavagnac, V., Monnin, C., Ceuleneer, G., Boulart, C., Hoareau, G., 2013b. Characterization of hyperalkaline fluids produced by low-temperature serpentinization of mantle peridotites in the Oman and Ligurian ophiolites. G-cubed 14. https://doi.org/10.1002/ggge.20147.
Cipolli, F., Gambardella, B., Marini, L., Ottonello, G., Zuccolini, M.V., 2004. Geochemistry of high-pH waters from serpentinites of the Gruppo di Voltri (Genova, Italy) and reaction path modeling of CO_2 sequestration in serpentinite aquifers. Appl. Geochem. 19, 787–802.
Claes, H., Softe, J., Van Noten, K., El Desouky, H., Erthal, M.M., Vanhaecke, F., Özkul, M., Swennen, R., 2015. Sedimentology, three-dimensional geobody reconstruction and carbon dioxide origin of Pleistocene travertine deposits in the Ballık area (south-west Turkey). Sedimentology 62, 1408–1445.
Claes, H., Erthal, M.M., Soete, J., Özkul, M., Swennen, R., 2017. Shrub and pore type classification: petrography of travertine shrubs from the Ballık-Belevi area (Denizli, SW Turkey). Quat. Int. 437, 147–163.
Claes, H., Huysmans, M., Soete, J., Dirix, K., Vassilieva, E., Marques Erthal, M., Vandewijngaerde, W., Hamaekers, H., Aratman, C., Özkul, M., Swennen, R., 2019. Elemental geochemistry to complement stable isotope data of fossil travertine: importance of digestion method and statistics. Sediment. Geol. 386, 118–131.
Clark, I.D., Fontes, J.-C., 1990. Paleoclimatic reconstruction in northern Oman based on carbonates from hyperalkaline groundwaters. Quat. Res. (Tokyo) 33, 320–336.
Clark, I.D., Fontes, J.-C., Fritz, P., 1992. Stable isotope disequilibria in travertine from high pH waters: laboratory investigations and field observations from Oman. Geochem. Cosmochim. Acta 56, 2041–2050.
De Baar, H.J.W., Schijf, J., Byrne, R.H., 1991. Solution chemistry of the rare earth elements in seawater. Eur. J. Solid State Inorg. Chem. 28, 357–373.
D'Alessandro, W., Daskalopoulou, K., Calabrese, S., Bellomo, S., 2018. Water chemistry and abiogenic methane content of a hyperalkaline spring related to serpentinization in the Argolida ophiolite (Ermioni, Greece). Mar. Petrol. Geol. 89, 185–193.
Elderfield, H., Sholkovitz, E.R., 1987. Rare earth elements in the pore waters of reducing nearshore sediments. Earth Planet Sci. Lett. 82, 280–288.
Elderfield, H., Upstill-Goddard, R., Sholkovitz, E.R., 1990. The rare earth elements in rivers, estuaries, and coastal seas and their significance to the composition of ocean waters. Geochem. Cosmochim. Acta 54, 971–991.
Etiope, G., Vadillo, I., Whiticar, M.J., Marques, J.M., Carreira, P.M., Tiago, I., Benavente, J., Jiménez, P., Urresti, B., 2016. Abiotic methane seepage in the Ronda peridotite massif, southern Spain. Appl. Geochem. 66, 101–113.
Flügel, E., 2004. Microfacies of Carbonate Rocks. Springer, Berlin, Heidelberg. https://doi.org/10.1007/978-3-662-08726-8_.
Fouke, B.W., Farmer, J.D., Des Marais, D.J., Pratt, L., Sturchio, N.C., Burns, P.C., Discipulo, M.K., 2000. Depositional facies and aqueous-solid geochemistry of travertine-depositing hot springs (Angel Terrace, Mammoth hot springs, Yellowstone National Park, USA). J. Sediment. Res. 70, 565–585.
Fowler, A.P.G., Zierenberg, R.A., Reed, M.H., Palandri, J., Óskarsson, F., Gunnarsson, I., 2019. Rare earth element systematics in boiled fluids from basalt-hosted geothermal systems. Geochem. Cosmochim. Acta 244, 129–154.
Gammon, C.H., Wood, S.A., Williams-Jones, A.E., 1996. The aqueous geochemistry of the rare earth elements and yttrium: VI. Stability of neodymium chloride complexes from 25 to 300°C. Geochem. Cosmochim. Acta 60, 4615–4630.
Gandin, A., Capezzuoli, E., 2014. Travertine: distinctive depositional fabrics of carbonates from thermal spring systems. Sedimentology 61, 264–290.

Garrido, C.J., Gueydan, F., Booth-Rea, G., Percigout, J., Hidas, K., Padron-Navarta, J.A., Marchesi, C., 2011. Garnet lherzolite and garnet-spinel mylonite in the Ronda peridotite: vestiges of Oligocene backarc mantle lithospheric extension in the western Mediterranean. Geology 39, 927–930.
Giampouras, M., Garrido, C.J., Zwicker, J., Vadillo, I., Smrzka, D., Bach, W., Peckmann, J., Jiminez, P., Benavente, J., Garcia-Ruiz, J.M., 2019. Geochemistry and mineralogy of serpentinization-driven hyperalkaline springs in the Ronda peridotites. Lithos 350–351, 105215.
Giampouras, M., Garrido, C.J., Bach, W., Los, C., Fussmann, D., Monien, P., Garcia-Ruiz, J.M., 2020. On the controls of mineral assemblages and textures in alkaline springs, Samail Ophiolite, Oman. Chem. Geol. 533, 119435.
Glombitza, C., Putman, L.I., Rempfert, K.R., Kubo, M.D., Schrenk, M.O., Templeton, A.S., Hoehler, T.M., 2021. Active microbial sulfate reduction in fluids of serpentinizing peridotites of the continental subsurface. Comm. Earth Environ. 2 https://doi.org/10.1038/s43247-021-00157-z.
Guillong, M., Horn, I., Günther, D., 2003. A comparison of 266 nm, 213 nm and 193 nm produced from a single solid state N:YAG laser for laser ablation ICP-MS. J. Anal. At. Spectrom. 18, 1224–1230.
Günther, D., Heinrich, C.A., 1999. Comparison of the ablation behaviour of 266 nm Nd:YAG and 193 nm ArF excimer lasers for LA-ICP-MS analysis. J. Anal. At. Spectrom. 14, 1369–1374.
Guo, L., Riding, R., 1992. Aragonite laminae in hot water travertine crusts. Rapolano Terme, Italy. Sedimenology 39, 1067–1079.
Haas, J.R., Shock, E.L., Sassani, D.C., 1995. Rare earth elements in hydrothermal systems: estimates of standard partial molal thermodynamic properties of aqueous complexes of the rare earth elements at high pressures and temperatures. Geochem. Cosmochim. Acta 59, 4329–4350.
Jochum, K.P., Weis, U., Stoll, B., Kuzmin, D., Yang, Q., Raczek, I., Jacob, D.E., Stracke, A., Birbaum, K., Frick, D.A., Günther, D., Enzweiler, J., 2011. Determination of reference values for NIST SRM 610-617 glasses following ISO guidelines. Geostand. Geoanal. Res. 35, 397–429.
Jochum, K.P., Scholz, D., Stoll, B., Weis, U., Wilson, S.A., Yang, Q., Schwalb, A., Börner, N., Jacob, D.E., Andraea, M.O., 2012. Accurate trace element analysis of speleothems and biogenic calcium carbonates by LA-ICP-MS. Chem. Geol. 318–319, 31–44.
Johannesson, K.H., Lyons, W.B., 1994a. The rare earth element geochemistry of Mono Lake water and the importance of carbonate complexing. Limnol. Oceanogr. 39, 1141–1154.
Johannesson, K.H., Lyons, W.B., Bird, D.A., 1994b. Rare earth element concentrations and speciations in alkaline lakes from the western USA. Geophys. Res. Lett. 21, 773–776.
Kelemen, P.B., Matter, J., Streit, E.E., Rudge, J.F., Curry, W.B., Blusztajn, J., 2011. Rates and mechanisms of mineral carbonation in peridotite: natural processes and recipes for enhanced, in situ CO_2 capture and storage. Annu. Rev. Earth Planet Sci. 39, 545–576.
Kelley, D.S., Karson, J.A., Früh-Green, G.L., Yoerger, D.R., Shank, T.A., Butterfield, D.A., Hayes, J.M., Schrenk, M.O., Olson, E.J., Proskurowski, G., Jakuba, M., Bradley, A., Larson, B., Ludwig, K., Glickson, D., Buckman, K., Bradley, A.S., Brazelton, W.J., Roe, K., Elend, M.J., Delacour, A., Bernasconi, S.M., Lilley, M.D., Baross, J.A., Summons, R.E., Sylva, S.P., 2005. A serpentinite-hosted ecosystem: the lost city hydrothermal field. Science 307, 1428–1434.
Kelly, S.D., Newville, M.G., Cheng, L., Kemner, K.M., Sutton, S.R., Fenter, P., Sturhcio, N.C., Spötl, C., 2003. Uranyl incorporation in natural calcite. Environ. Sci. Technol. 37, 1284–1287.
Khoury, H.N., Salameh, E.M., Clark, I.D., 2014. Mineralogy and origin of surficial uranium deposits hosted in travertine and calcrete from central Jordan. Appl. Geochem. 43, 49–65.
Klein, F., McCollom, T.M., 2013. From serpentinization to carbonation: new insights from a CO_2 injection experiment. Earth Planet Sci. Lett. 379, 137–145.
Lécuyer, C., Reynard, B., Grandjean, P., 2004. Rare earth element evolution of Phanerozoic seawater recorded in biogenic apatites. Chem. Geol. 204, 63–102.
Lee, J.H., Byrne, R.H., 1993. Rare earth element complexation by fluoride ions in aqueous solution. J. Solut. Chem. 22, 751–766.
Lenoir, X., Garrido, C.J., Bodinier, J.-L., Dautria, J.-M., Gervilla, F., 2001. The recrystallization front of the Ronda Peridotite: evidence for melting and thermal erosion of subcontinental lithospheric mantle beneath the Alboran Basin. J. Petrol. 42, 141–158.
Leybourne, M.I., Goodfellow, W.D., Boyle, D.R., Hall, G.M., 2000. Rapid development of negative Ce anomalies in surface waters and contrasting REE patterns in groundwaters associated with Zn – Pb massive sulphide deposits. Appl. Geochem. 15, 695–723.
Li Vigni, L., Daskalopoulou, K., Calabrese, S., Parello, F., D'Alessandro, W., 2021. Geochemical characterisation of the alkaline and hyperalkaline groundwater in the Othrys Ophiolite Massif, central Greece. Ital. J. Geosci. 140, 42–56.
Luo, Y.-R., Byrne, R.H., 2001. Yttrium and rare earth element complexation by chloride ions at 25°C. J. Solut. Chem. 30, 837–845.
Luo, Y.-R., Byrne, R.H., 2004. Carbonate complexation of yttrium and the rare earth elements in natural waters. Geochem. Cosmochim. Acta 68, 691–699.
McCollom, T.M., Seewald, J.S., 2013. Serpentinites, hydrogen, and life. Elements 9, 129–134.
McLennan, S.M., 1989. Rare earth elements in sedimentary rocks; influence of provenance and sedimentary processes. Rev. Mineral. Geochem. 21, 169–200.
Mervine, E.M., Humphris, S.E., Sims, K.W.W., Kelemen, P.B., Jenkins, W.J., 2014. Carbonation rates of peridotite in the Samail Ophiolite, Sultanate of Oman, constrained through ^{14}C dating and stable isotopes. Geochem. Cosmochim. Acta 126, 371–397.
Meyer-Dombard, D.R., Woycheese, K.M., Yargicoglu, E.N., Cardace, D., Shock, E.L., Gülecal-Pektas, Y., Temel, M., 2015. High pH microbial ecosystems in a newly discovered, ephemeral, serpentinizing fluid seep at Yanartaş (Chimera), Turkey. Front. Microbiol. 5 https://doi.org/10.3389/fmicb.2014.00723 article 723.
Migdisov, A.A., Williams-Jones, A.E., 2008. A spectrophotometric study of Nd(III), Sm (III) and Er(III) complexation in sulfate-bearing solutions at elevated temperatures. Geochem. Cosmochim. Acta 72, 5291–5303.
Migdisov, A.A., Williams-Jones, A.E., 2014. Hydrothermal transport and deposition of the rare earth elements by fluorine-bearing aqueous liquids. Miner. Deposita 49, 987–997.
Migdisov, A.A., Williams-Jones, A.E., Wagner, T., 2009. An experimental study of the solubility and speciation of the REE (III) in fluoride- and chloride-bearing aqueous solutions at temperatures up to 300°C. Geochem. Cosmochim. Acta 73, 7087–7109.
Miller, H.M., Matter, J.M., Kelemen, P., Ellison, E.T., Conrad, M.E., Fierer, N., Ruchala, T., Tominaga, M., Templeton, A.S., 2016. Modern water/rock reactions in Oman hyperalkaline peridotite aquifers and implications for microbial habitability. Geochem. Cosmochim. Acta 179, 217–241.
Moffett, J.W., 1990. Microbially mediated cerium oxidation in seawater. Nature 345, 421–423.
Möller, P., Bau, M., 1993. Rare-earth patterns with positive cerium anomaly in alkaline waters from Lake Van, Turkey. Earth Planet Sci. Lett. 117, 671–676.
Morrill, P.L., Brazelton, W.S., Kohl, L., Rietze, A., Miles, S.M., Kavanagh, H., Schrenk, M.O., Ziegler, S.E., Lang, S.Q., 2014. Investigations of potential microbial methanogenic and carbon monoxide utilization pathways in ultra-basic reducing springs associated with present-day continental serpentinization: the Tablelands, NL, CAN. Front. Microbiol. 5 article 613.
Neal, C., Shand, P., 2002. Spring and surface water quality of the Cyprus ophiolites. Hydrol. Earth Syst. Sci. 6, 797–817.
Neal, C., Stanger, G., 1984. Calcium and magnesium hydroxide precipitation from alkaline groundwaters in Oman, and their significance to the process of serpentinization. Mineral. Mag. 48, 237–241.
Neal, C., Stanger, G., 1985. Past and present serpentinization of ultramafic rocks: an example from the Semail ophiolite nappe of northern Oman. In: Drewer, J.I. (Ed.), The Chemistry of Weathering. D. Reidel Publishing Company, Holland, pp. 249–275.
Nothdurft, L.D., Webb, G.E., Kamber, B.S., 2004. Rare earth element geochemistry of Late Devonian reefal carbonates, Canning Basin, Western Australia: confirmation of a seawater REE proxy in ancient limestones. Geochem. Cosmochim. Acta 68, 263–283.
Olsson, J., Stipp, S.L.S., Gislason, S.R., 2014. Element scavenging by recently formed travertine deposits in the alkaline springs from the Oman Semail Ophiolite. Mineral. Mag. 78, 1479–1490.
Parekh, P.P., Möller, P., Dulski, P., 1977. Distribution of trace elements between carbonate and non-carbonate phases of limestone. Earth Planet Sci. Lett. 34, 39–50.
Paukert, A.N., Matter, J.M., Kelemen, P.B., Shock, E.L., Havig, J.R., 2012. Reaction path modeling of enhanced in situ CO_2 mineralization for carbon sequestration in the peridotite of the Samail Ophiolite, Sultanate of Oman. Chem. Geol. 330–331, 86–100.
Platt, J.P., Argles, T.W., Carter, A., Kelley, S.P., Whitehouse, M.J., Lonergan, L., 2003. Exhumation of the Ronda peridotite and its crustal envelope: constraints from thermal modelling of a P–T–time array. J. Geol. Soc. Lon. 160, 655–676.
Pourret, O., Davranche, M., Gruau, G., Dia, A., 2008. New insights into cerium anomalies in organic-rich alkaline waters. Chem. Geol. 251, 120–177.
Reeder, R.J., Lamble, G.M., Northrup, P.A., 1999. XAFS study of the coordination and local relaxation around Co^{2+}, Zn^{2+}, Pb^{2+}, and Ba^{2+} trace elements in calcite. Am. Mineral. 84, 1049–1060.
Reeder, R.J., Nugent, M., Lamble, G.M., Tait, C.D., Morris, D.E., 2000. Uranyl incorporation into calcite and aragonite: XAFS and luminescence studies. Environ. Sci. Technol. 34, 638–644.
Russell, M.J., Hall, A.J., Martin, W., 2010. Serpentinization as a source of energy at the origin of life. Geobiology 8, 355–371.
Schier, K., Himmler, T., Lepland, A., Kraemer, D., Schönenberger, J., Bau, M., 2021. Insights into the REY inventory of seep carbonates from the Northern Norwegian margin using geochemical screening. Chem. Geol. 559, 119857.
Schijf, J., Byrne, R.H., 2001. Stability constants for mono- and dioxalato-complexes of Y and the REE, potentially important species in groundwaters and surface freshwaters. Geochem. Cosmochim. Acta 65, 1037–1046.
Schijf, J., Christenson, E.A., Byrne, R.H., 2015. YREE scavenging in seawater: a new look at an old model. Mar. Chem. 177, 460–471.
Schmidt, K., Bau, M., Merschel, G., Tepe, N., 2019. Anthropogenic gadolinium in tap water and in tap water-based beverages from fast-food franchises in six major cities in Germany. Sci. Total Environ. 687, 1401–1408.
Schwarzenbach, E.M., Früh-Green, G.L., Bernasconi, S.M., Alt, J.C., Plas, A., 2013a. Serpentinization and carbon sequestration: a study of two ancient peridotite-hosted hydrothermal systems. Chem. Geol. 351, 115–133.
Schwarzenbach, E.M., Lang, S.Q., Früh-Green, G.L., Lilley, M.D., Bernasconi, S.M., Méhay, S., 2013b. Sources and cycling of carbon in continental, serpentinite-hosted alkaline springs in the Voltri Massif, Italy. Lithos 177, 226–244.
Serrano, M.J.G., Auque, S.L.F., Nordstrom, D.K., 2000. REE speciation in low-temperature acidic waters and the competitive effects of aluminum. Chem. Geol. 165, 167–180.
Sholkovitz, E.R., Shen, G.T., 1995. The incorporation of rare earth elements in modern coral. Geochem. Cosmochim. Acta 59, 2749–2756.
Sholkovitz, E.R., Landing, W.M., Lewis, B.L., 1994. Ocean particle chemistry: the fractionation of rare earth elements between suspended particles and seawater. Geochem. Cosmochim. Acta 58, 1567–1579.

Smrzka, D., Zwicker, J., Bach, W., Feng, D., Himmler, T., Chen, D., Peckmann, J., 2019. The behavior of trace elements in seawater, sedimentary pore water, and their incorporation into carbonate minerals: a review. Facies 65, 1–47.
Smrzka, D., Feng, D., Himmler, T., Zwicker, J., Hu, Y., Monien, P., Tribovillard, N., Chen, D., Peckmann, J., 2020. Trace elements in methane-seep carbonates: potentials, limitations, and perspectives. Earth Sci. Rev. 208, 103263.
Somasundaran, P., Agar, G.E., 1967. The zero point of charge of calcite. J. Colloid Interface Sci. 24, 433–440.
Sturchio, N.C., Antonio, M.R., Soderholm, L., Sutton, S.R., Brannon, J.C., 1998. Tetravalent uranium in calcite. Science 281, 971–973.
Suen, C.J., Frey, F.A., 1987. Origins of the mafic and ultramafic rocks in the Ronda peridotite. Earth Planet Sci. Lett. 85, 183–202.
Szponar, N., Brazelton, W.J., Schrenk, M.O., Bower, D.M., Steele, A., Morrill, P.L., 2013. Geochemistry of a continental site of serpentinization in the tablelands ophiolite, gros morne national park: a mars analogue. Icarus 224, 286–296.
Tang, J., Johannesson, K.H., 2003. Speciation of rare earth elements in natural terrestrial waters: assessing the role of dissolved organic matter from the modeling approach. Geochem. Cosmochim. Acta 67, 2321–2339.
Teboul, P.-A., Durlet, C., Gaucher, E.C., Virgone, A., Girard, J.-P., Curie, J., Lopez, B., Camoin, G.F., 2016. Origins of elements building travertine and tufa: new perspectives provided by isotopic and geochemical tracers. Sediment. Geol. 334, 97–114.
Templeton, A.S., Ellison, E.T., Glombitza, C., Morono, Y., Rempfert, K.R., Hoehler, T., Zeigler, S.D., Kraus, E., Spear, J., Nothaft, D., Fones, E.M., Boyd, E., Munro-Ehrlich, M., Mayhew, L., Cardace, D., Matter, J., Kelemen, P.B., 2021. Accessing the subsurface biosphere within rocks undergoing active low-temperature serpentinization in the Samail ophiolite (Oman Drilling Project). JGR Biogeosciences 126, e2021JG006315 the Oman Drilling Project Science Party.
Tribovillard, N., Algeo, T.J., Lyons, T., Riboulleau, A., 2006. Trace metals as paleoredox and paleoproductivity proxies: an update. Chem. Geol. 232, 12–32.
Tubia, J.M., Cuevas, J., Gil Ibarguchi, J.I., 1997. Sequential development of the metamorphic aureole beneath the Ronda peridotites and its bearing on the tectonic evolution of the Betic Cordillera. Tectonophysics 279, 227–252.
Vadillo, I., Urresti, B., Jiménez-Gavilán, P., Martos-Rosillo, S., Durán, J.J., Benavente, J., Carrasco, F., Pedrera, A., 2015. Preliminary hydrochemical characterization of Ronda peridotite massif (Málaga province). El Agua en Andalucía: El agua, clave medioambiental y socioeconómica, pp. 515–525.
Van der Waal, D., Vissers, R.L.M., 1996. Structural petrology of the Ronda peridotite, SW Spain: deformation history. J. Petrol. 37, 23–43.
Webb, G.E., Kamber, B.S., 2000. Rare earth elements in Holocene reefal microbialites: a new shallow seawater proxy. Geochem. Cosmochim. Acta 64, 1557–1565.
Winkel, L.H.E., Casentini, B., Bardelli, F., Voegelin, A., Nikolaidis, N.P., Charlet, L., 2013. Speciation of arsenic in Greek travertines: Co-precipitation of arsenate with calcite. Geochem. Cosmochim. Acta 106, 99–110.
Wood, S.A., 1990. The aqueous geochemistry of the rare-earth elements and yttrium 1. Review of available low-temperature data for inorganic complexes and the inorganic REE speciation of natural waters. Chem. Geol. 82, 159–186.
Zhang, J., Nozaki, Y., 1998. Behavior of rare earth elements in seawater at the ocean margin: a study along the slopes of the Sagami and Nankai troughs near Japan. Geochem. Cosmochim. Acta 62, 1307–1317.
Zhao, M.-Y., Zheng, Y.-F., 2014. Marine carbonate records of terrigenous input into Paleotethyan seawater: geochemical constraints from Carboniferous limestones. Geochem. Cosmochim. Acta 141, 508–531.
Zwicker, J., Birgel, D., Bach, W., Richoz, S., Smrzka, D., Grasemann, B., Gier, S., Schleper, C., Rittmann, S.K.-M.R., Kosun, E., Peckmann, J., 2018a. Evidence for archaeal methanogenesis within veins at the onshore serpentinite-hosted Chimaera seeps, Turkey. Chem. Geol. 483, 567–580.
Zwicker, J., Smrzka, D., Himmler, T., Monien, P., Gier, S., Goedert, J.L., Peckmann, J., 2018b. Rare earth elements as tracers for microbial activity and early diagenesis: a new perspective from carbonate cements of ancient methane-seep deposits. Chem. Geol. 501, 77–85.